Hindawi
Structural Control and Health Monitoring
Volume 2023, Article ID 8234927, 26 pages
https://doi.org/10.1155/2023/8234927

Research Article

A Cross-Diagnosis Method for Determining the Structural Condition of a Long-Span Suspension Bridge Based on the Spatial Windows of Distributed Strain Data

Qianen Xu, Zheng Zhou, and Yang Liu

School of Transportation Science and Engineering, Harbin Institute of Technology, Harbin 150090, China

Correspondence should be addressed to Yang Liu; ly7628@hit.edu.cn

Received 28 March 2023; Revised 15 June 2023; Accepted 22 June 2023; Published 27 July 2023

Academic Editor: Jun Li

Using structural health monitoring (SHM) techniques, Brillouin optical time-domain analysis (BOTDA) sensors can be mounted along the main box girder entire length of a long-span suspension bridge, and the high-density measured points strain monitoring data can be obtained. However, insufficient research has been conducted on accurately diagnosing the structural condition of a long-span suspension bridge by using the abovementioned strain monitoring data. To address this issue, a cross-diagnosis method that determines the structural condition of long-span suspension bridges based on the distributed strain data spatial window is proposed in this study. First, the distributed strain data spatial window based on a long-span suspension bridge structural symmetry is defined. Then, a method that divides the distributed strain data of the bridge main box girder into different spatial windows using mutual information between the strain data from BOTDA sensors is presented. The special symmetry of the environmental temperature effect on the spatial window structural performance is carried out to separate the temperature effect from the strain monitoring data; this process can effectively reduce the interference of ambient temperature on the results of the structural condition diagnosis. Second, using a convolutional neural network, a diagnosis index of the structural condition is generated by using the correlation model between the high-density measured points and the distributed strain data belonging to one whole spatial window. Regarding one spatial window, the proposed diagnosis index can effectively reflect the variation in the distributed strain correlation model caused by the damaged condition of the long-span suspension bridge to achieve cross-diagnosis of the structural condition of the bridge. Finally, the effectiveness of the proposed method is demonstrated through a numerical simulation using strain monitoring data obtained from a real bridge.

1. Introduction

In recent years, structural health monitoring for bridge structures has received increasing attention because it can continuously monitor bridge structures and collect long-term structural and environmental monitoring data [1–3]. Many scholars have studied the monitoring data provided by bridge structural health monitoring systems to diagnose the conditions of bridge structures [4]. According to the different sensor types, monitoring data provided by the bridge structural health monitoring system can be divided into vibration acceleration data, strain data, displacement data, and so on. Vibration acceleration data are considered effective data [5], and the methods of diagnosing conditions of bridge structures by using bridge dynamic characteristics have been extensively studied [6–11]. Regarding static data of bridge structures, such as strain and displacement data, the method for constructing condition diagnosis indexes of bridge structures based on the correlation model between the monitoring data is widely used [12, 13]. In addition, based on the diagnostic methods of a single bridge, methods for diagnosing bridge structure conditions using monitoring data of bridges monitored within one cluster have also been studied [14–17].

Although many scholars have studied how to effectively use the monitoring data of various bridge structures for long-span bridge structures, which are particularly affected by environmental temperature, removing the influence of

environmental temperature in the bridge structure monitoring data is still a key problem in the process of diagnosing the long-span bridge structure conditions [18]. To solve the above problems, some scholars have carried out relevant studies examining the correlation between the responses of bridge structures and the ambient temperature and the diagnosis indexes of bridge structure conditions independent of the ambient temperature. In the study of the correlation between the structural response of bridges and ambient temperature, the analysis of finite element model data and real bridges, machine learning, and other methods have been widely used. Farreras-Alcover et al. [19] established a correlation model of the strain and temperature of steel bridge panels welded joints by using a regression analysis method and diagnosed the welded joints structural conditions based on the correlation model. Zhou and Sun [20, 21] used the actual monitoring data of a cable-stayed bridge to analyze the correlation between the structural response (displacement, cable tensions, strain, and so on) of the cable-stayed bridge and ambient temperature, providing guidance for reducing the influence of ambient temperature on the diagnosis results of bridge conditions. Buckley et al. [22] used a dynamic harmonic regression time-series model to model recorded temperature values and strain data. Lei et al. [23] used a residual autoencoder model to establish the correlation between the ambient temperature and displacement response of long-span cable-stayed bridges. Regarding constructing the structural condition diagnosis indexes for bridges that are not affected by ambient temperature, various methods that utilize either a single type of structural response or multiple types of structural responses have been proposed. Deraemaeker and Worden [24] constructed feature vectors to remove environmental impacts based on the Mahalanobis distance. Soo Lon Wah et al. [25] used the principal component analysis method to process monitoring data and distinguished the influence of structural damage and environmental factor changes on the monitoring data. Fallahian et al. [26] proposed a method that determines the condition diagnosis of bridge structures based on pattern recognition in combination with coupled sparse coding and a deep neural network. This method can diagnose structural conditions in the presence of uncertain factors such as noise and temperature. Erazo et al. [27] proposed a structural condition diagnosis method based on Kalman filtering under changing environmental conditions and constructed the structural damage diagnosis index based on the spectral moments of the residual spectral density. Xu et al. [28] built a correlation model between the deflection of girders and tension in cables based on an unsupervised deep learning network and then used this model to construct the diagnosis indexes of bridge structure conditions.

In the above studies, point sensors are mostly used, but the number of measured points is small. Recent advances in distributed optical fiber sensing technology provide strong support for solving the above problems. The principle of distributed optical fiber sensing technology is to use the characteristics of the backscattering effect in the fibers, as such an effect is sensitive to external physical quantities such as temperature or strain; moreover, distributed optical fiber sensing technology obtains the measurements of external physical quantities over the entire lengths of the fibers through the measurement of the backscattering light signal [29]. In recent years, to improve the performance index of distributed optical fiber sensing technology in terms of spatial resolutions, measurement speeds and measurement distances, optimizing differential pulse-width pair Brillouin optical time-domain analysis, fast-scanning Brillouin gain spectra, and other technologies have been developed [30–32]. Due to the advantages of convenient installation, strong durability, and immunity to electromagnetic interference, distributed optical fiber sensing technology has received extensive attention in the application of bridge structure monitoring [33–35]. However, regarding the use of distributed optical fiber monitoring data to diagnose conditions of long-span bridge structures, current research is relatively limited. Zhang et al. [36] used the bridge structure distributed strain data to construct a strain space-time matrix and used it to characterize the structural damage behavior and damage evolution mode. Wei et al. [37] studied the spatial-temporal features of distributed strain under vehicle load and then determined vehicle load events by using measured data to eliminate the influences of vehicle loads on the diagnosis of bridge structure conditions. Scarella et al. [38] established a relationship between the redistribution of deck strains and the tension loss in the individual cables of cable-stayed bridges by using distributed dynamic strain sensing technology. Oskoui et al. [39] proposed a bridge damage detection method without reference measurements by using dynamically distributed optical fibers. In addition, regarding the problem that the strain of the fiber core is inconsistent with the structural strain caused by the cable protective layer and surface sticking, some scholars have proposed methods for calculating the strain transfer coefficient through theoretical research, numerical simulation, and experimental research [40–44].

Compared with point sensors, distributed optical fiber sensors can provide strain monitoring data for high-density measured points; as such data contain more information on the conditions of bridge structures [45, 46]. In addition, local load and other factors can only affect the strain monitoring data of a small part of the measured points at a single point in time, so the distributed strain obtained can reflect the response of the overall structure with long-term temperature change. Therefore, using the monitoring data of the distributed optical fiber sensors, the problem of local damage being ignored can be avoided, and the diagnosis of the structural condition can be realized more effectively. To effectively use the strain monitoring data of high-density measured points, it is necessary to consider the combined application of monitoring data of the different measuring points. However, at present, research on using distributed strain data to achieve structural condition diagnosis of long-span suspension bridges is insufficient. Moreover, the distributed strain data of long-span suspension bridges are greatly affected by the environment, and the variation in structural conditions is easy to cover. Therefore, using a reasonable method to process the distributed strain monitoring data at different locations of a long-span

suspension bridge and to reduce the interference of ambient temperature on the results of the structural condition diagnoses for long-span suspension bridges is still a key issue. To address this issue, a cross-diagnosis method that determines the structural condition of a long-span suspension bridge based on the spatial windows of distributed strain data are proposed. First, the spatial window of distributed strain data based on the structural symmetry of a long-span suspension bridge is defined in Section 2; then, a method that divides the distributed strain data of entire main bridge box girders into different spatial windows by using the mutual information between the strain data from BOTDA sensors is presented. Next, using a convolutional neural network, a diagnosis index of the structural condition is generated through a correlation model between the distributed strain data of high-density measured points belonging to one whole spatial window in Section 3. Finally, the effectiveness of the proposed method is demonstrated by using a numerical simulation and strain monitoring data obtained from a real bridge.

2. Division of the Spatial Windows Based on the Mutual Information between the Distributed Strain Data

2.1. Definition of the Spatial Window of Distributed Strain Data. Regarding the main girder structures of long-span suspension bridges, it is assumed that there is a strain measured at point A (as shown in Figure 1), and the strain of the structure at this point is subject to the coupling effect of vehicle load, environmental temperature, and other factors, and this relationship can be expressed as follows:

$$U_A(t) = f_V(\mathbf{V}(t)) + f_T(\mathbf{T}(t)) + \theta_A(t), \tag{1}$$

where $U_A(t)$ is the structural strain response at Point A changing over time t, $\mathbf{V}(t)$ is the vehicle load vector changing over time t, $\mathbf{T}(t)$ is the environmental temperature vector changing over time t, $f_V(\mathbf{V}(t))$ is the structural strain at Point A caused by vehicle load $\mathbf{V}(t)$, $f_T(\mathbf{T}(t))$ is the structural strain at Point A caused by environmental temperature $\mathbf{T}(t)$, and $\theta_A(t)$ is the structural strain at Point A caused by other loads.

As shown in Figure 1, since the influence of ambient temperature is similar at the symmetrical position of the bridge, the structural strain of the measured point A under a temperature load and Point A' is considered symmetric with the strain measured point A of the main girder, and it has the following correlation:

$$f_T'(\mathbf{T}(t)) = f_{\mathrm{AA}'}\left(f_T(\mathbf{T}(t))\right), \tag{2}$$

where $f_{\mathrm{AA}'}(\cdot)$ is the correlation between the structural strain of measured points A and A' caused by the ambient temperature and $f_T'(\mathbf{T}(t))$ is the structural strain of measured point A' caused by the ambient temperature.

Using equations (1) and (2), the structural strain of measured point A' can be expressed by the following equation:

$$U_{A'}(t) = f_V'(\mathbf{V}(t)) + f_{\mathrm{AA}'}\left(f_T(\mathbf{T}(t))\right) + \theta_{A'}(t), \tag{3}$$

where $f_V'(\mathbf{V}(t))$ is the structural strain of measured point A' caused by a vehicle load, $\theta_A'(t)$ is the structural strain response of measured point A' caused by other loads, and $U_{A'}(t)$ is the structural strain response of measured point A' changing over time t.

Equations (1) to (3) are combined to yield

$$\begin{aligned} U_{A'}(t) - f_{\mathrm{AA}'}\left(U_A(t)\right) &= U_{A'}(t) - f_{\mathrm{AA}'}\left(f_V(\mathbf{V}(t)) + f_T(\mathbf{T}(t)) + \theta_A(t)\right) \\ &= U_{A'}(t) - f_{\mathrm{AA}'}\left(f_V(\mathbf{V}(t))\right) - f_{\mathrm{AA}'}\left(f_T(\mathbf{T}(t))\right) - f_{\mathrm{AA}'}\left(\theta_A(t)\right) \\ &= f_V'(\mathbf{V}(t)) - f_{\mathrm{AA}'}\left(f_V(\mathbf{V}(t))\right) + \theta_{A'}(t) - f_{\mathrm{AA}'}\left(\theta_A(t)\right) \\ &= f\left(\mathbf{V}(t), \theta_{A'}(t), \theta_A(t)\right), \end{aligned} \tag{4}$$

where $f(\mathbf{V}(t), \theta_{A'}(t), \theta_A(t))$ is the function with $\mathbf{V}(t)$, $\theta_{A'}(t)$, and $\theta_A(t)$ as the independent variables.

Regarding real bridges, vehicle loads and other loads can be regarded as random variables. Therefore, $f(\mathbf{V}(t), \theta_{A'}(t), \theta_A(t))$ in equation (4) can be considered as the residual of the correlation model between the structural strain monitoring data at measured point A and measured point A'. Ambient temperature effects are no longer included in the above residuals. Therefore, the establishment of the strain correlation model between measured point A and its symmetric measured point A' can eliminate the influence of ambient temperature on the strain monitoring data, thus providing a basis for the establishment of structural condition diagnosis indexes for long-span suspension bridges. Regarding the structural health monitoring system of a real bridge, construction errors inevitably exist in the process of mounting distributed optical fibers. Therefore, by considering the data of measured points close to the measured points A or A', the correlation between the strain monitoring data of the measured points in the symmetrical area of the bridge can be established to eliminate the influence of ambient temperature, as described by the following three equations:

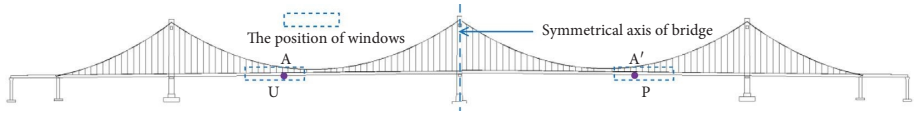

Figure 1: Sketch diagrams of the spatial windows of long-span suspension bridges.

$$\mathbf{U}_{A'}(t) - f_{\mathbf{U}_A\mathbf{U}_{A'}}(\mathbf{U}_A(t)) = \mathbf{f}(\mathbf{V}(t), \theta_{A'}(t), \theta_A(t), \theta_{A'-1}(t), \theta_{A-1}(t), \theta_{A'+1}(t), \theta_{A+1}(t), \ldots), \tag{5}$$

$$\mathbf{U}_{A'}(t) = [\ldots, U_{A'-1}(t), U_{A'}(t), U_{A'+1}(t), \ldots], \tag{6}$$

$$\mathbf{U}_A(t) = [\ldots, U_{A-1}(t), U_A(t), U_{A+1}(t), \ldots], \tag{7}$$

where $\mathbf{U}_A(t)$ and $\mathbf{U}_{A'}(t)$ are the strain vectors of the measured points near measured point A or measured point A' which change over time t, respectively; $U_{A'-1}(t)$ and $U_{A'+1}(t)$ are the strain monitoring data of the adjacent point on the left and the adjacent point on the right of measured point A', which change over time t, respectively; $U_{A-1}(t)$ and $U_{A+1}(t)$ are the strain monitoring data of the adjacent point on the left and the adjacent point on the right of measured point A, which change over time t, respectively; $f_{\mathbf{U}_A\mathbf{U}_{A'}}(\cdot)$ is the correlation model between $\mathbf{U}_A(t)$ and $\mathbf{U}_{A'}(t)$ established by using the strain monitoring data, and $\mathbf{f}(\mathbf{V}(t), \theta_{A'}(t), \theta_A(t), \theta_{A'-1}(t), \theta_{A-1}(t), \theta_{A'+1}(t), \theta_{A+1}(t), \ldots)$ is the residual of the correlation model between $\mathbf{U}_A(t)$ and $\mathbf{U}_{A'}(t)$.

As seen from equations (5) to (7), the residual of the relevant model of the measured points strain monitoring data in the symmetrical area of the bridge is not affected by the ambient temperature. The residual can be used to construct the diagnosis index of the structural condition, thus reducing the interference of the ambient temperature on the diagnosis result of the structural condition. Therefore, the above symmetric areas of bridges can be defined as the spatial window, and such window can be used as the basis for further diagnosing structural conditions.

In summary, the spatial window of distributed strain data of a long-span suspension bridge is defined as follows. As shown in Figure 1, distributed optical fiber sensors are laid along the longitudinal length of the main girder, with symmetric local longitudinal Areas U and P of the main girder. Then, the spatial window of distributed strain data is the main girder area composed of Areas U and P, and the structural strain responses of the high-density measured points are contained in the spatial window.

2.2. Division of the Spatial Windows of Distributed Strain Data. The spatial window of distributed strain data is defined in Section 2.1, and the method for dividing the distributed strain data of the bridge entire main girder into different spatial windows is presented in this section. According to the definition of the spatial window, there is a significant correlation between the strain data of the main girder structure and the spatial window. The maximal information coefficient is a mathematical tool capable of effectively detecting data correlations. Therefore, the size evaluation index of the spatial window is constructed based on the maximal information coefficient by utilizing the symmetry of the measured points in the spatial window, and then a reasonable division for the spatial windows of distributed strain data are obtained.

The structurally distributed strain data of the left area and the right area of the rth spatial window at the ith monitoring time are defined as follows:

$$\begin{aligned} \mathbf{U}_i^r &= \left[U_{i1}^r, U_{i2}^r, \ldots, U_{\mathrm{ij}}^r, \ldots, U_{\mathrm{in}}^r\right]^{\mathrm{T}}, \\ \mathbf{P}_i^r &= \left[U'^r_{i1}, U'^r_{i2}, \ldots, U'^r_{\mathrm{ij}}, \ldots, U'^r_{\mathrm{in}}\right]^{\mathrm{T}}, \end{aligned} \tag{8}$$

where n is the total number of structural distributed strain measured points in the left area of the rth spatial window, U_{ij}^r is the measured structural strain data of the jth measured point in the left area of the rth spatial window at the ith monitoring time, U'^r_{ij} is the measured structural strain data of the jth measured point in the right area of the rth spatial window at the ith monitoring time, $\mathbf{U}_i^r$ is the structural distributed strain response vector of the left area of the rth spatial window at the ith monitoring time, and $\mathbf{P}_i^r$ is the structural distributed strain response vector in the right area of the rth spatial window at the ith monitoring time.

To calculate the maximal information coefficient of the measured points strain data in the spatial window, strain data of two different measured points at multiple times are selected to form a sample set, as shown in the following equations:

$$\begin{aligned} \mathbf{U}^{r,j} &= \left[U_{1j}^r; U_{2j}^r; \ldots\right], \\ \mathbf{P}^{r,h} &= \left[U'^r_{1h}; U'^r_{2h}; \ldots\right]^{\mathrm{T}}, \end{aligned} \tag{9}$$

where $\mathbf{U}^{r,j}$ is the strain data sample set of the jth measured point in the left area of the rth spatial window and $\mathbf{P}^{r,h}$ is the strain data sample set of the hth measured point in the right area of the rth spatial window.

The strain of the jth measured point in the left area of the spatial window is taken as the x-coordinate, and the strain of the hth measured point in the right area of the spatial window is taken as the y-coordinate. The above sample data are divided into Grid G of the a_u row and b_u column, and the coordinates of the data points in the grid are shown in equation (10). Grid G is shown in Figure 2.

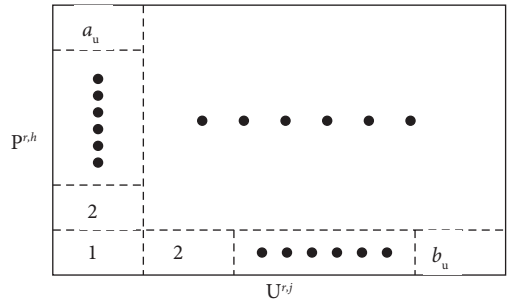

Figure 2: Grid G obtained from the strain data sample set.

$$\{\mathbf{X}_1, \mathbf{X}_2, \ldots\} = \left\{\left(U_{1j}^{r}, U'^{r}_{1h}\right), \left(U_{2j}^{r}, U'^{r}_{2h}\right), \ldots\right\}, \tag{10}$$

where $\mathbf{X}_1$ and $\mathbf{X}_2$ are the first and second data points in Grid G, respectively.

Then, the mutual information of the sample set when it is divided into Grid G can be calculated as follows:

$$I_{\mathrm{jh}}\left(G_{a_u,b_u}\right) = \sum\sum f(a_u, b_u)\log\left(\frac{f(a_u, b_u)}{f(a_u) f(b_u)}\right),$$
$$f(a_u, b_u) = \frac{n_{(a_u,b_u)}}{n_{\mathrm{all}}}, \tag{11}$$

where $n_{(a_u,b_u)}$ is the number of strain data points of the sample set in the a_uth row and b_uth column of the grid; n_{all} is the total number of data points of the sample set; $f(a_u, b_u)$ is the ratio of the number of strain data points in the a_uth row and b_uth column of Grid G to the total number of strain data points; and $f(a_u)$ and $f(b_u)$ are the marginal distributions of $f(a_u, b_u)$ in the x and y directions, respectively.

There are many ways to obtain Grid G, and the Grid G with the largest mutual information is selected. Hence, the mutual information $I_{\mathrm{jh}}(a_u, b_u)$ can be expressed by the following equation:

$$I_{\mathrm{jh}}(a_u, b_u) = \max\left(I_{\mathrm{jh}}\left(G_{a_u,b_u}\right)\right). \tag{12}$$

The mutual information of grids with different row and column numbers is calculated and normalized [47]. The greater the mutual information after normalization, the better the grid division is. The maximal information coefficient of the distributed strain data of the jth measured point and the hth measured point $\mathrm{MIC}_{\mathrm{jh}}$ is shown as follows:

$$\mathrm{MIC}_{\mathrm{jh}} = \max\left(\frac{I_{\mathrm{jh}}(a_u, b_u)}{\log_2 \min\left([a_u, b_u]\right)}\right). \tag{13}$$

According to the above equation, the maximal information coefficient of the strain data of different measured points in the left area and the right area in the rth spatial window can be developed into the following matrix:

$$\mathbf{M} = \begin{bmatrix} \mathrm{MIC}_{11} & \mathrm{MIC}_{12} & \cdots & \mathrm{MIC}_{1n} \\ \mathrm{MIC}_{21} & \mathrm{MIC}_{22} & & \\ \vdots & & \ddots & \vdots \\ \mathrm{MIC}_{n1} & & \cdots & \mathrm{MIC}_{\mathrm{nn}} \end{bmatrix}. \tag{14}$$

The higher the MIC is, the stronger the correlation of the strain of the measured points. Therefore, the size evaluation index of the spatial window can be constructed by using the following equation:

$$C = \frac{1}{n^2}\,\mathrm{sum}\left(\mathrm{diag}\left(\mathbf{MI}\right)\right), \tag{15}$$

$$\mathbf{I} = \begin{bmatrix} 1 & 1 & \cdots & 1 \\ 1 & 1 & & \\ \vdots & & \ddots & \vdots \\ 1 & & \cdots & 1 \end{bmatrix}_{n\times n}, \tag{16}$$

where $\mathrm{diag}(\cdot)$ represents extracting the main diagonal elements of the matrix as column vectors and $\mathrm{sum}(\cdot)$ represents calculating the sum of a vector.

Using the above size evaluation index of the spatial window, the specific steps of the division method for distributed strain data spatial windows of long-span suspension bridges are as follows:

(1) Regarding long-span suspension bridge structures, the initial size of the spatial window is the section area of the main girder between two suspenders along the longitudinal length of the bridge.

(2) The size evaluation index of the initial spatial window is calculated by using equation (15), and the result is denoted as C_{11}.

(3) The size of the spatial window is enlarged, and the expanded size can be the distance between measured points.

(4) The size evaluation index of the spatial window that was determined in Step (iii) is calculated by using equation (15), and the result is denoted as C_{12}.

(5) If $C_{12} > C_{11}$, it is determined that $C_{11} = C_{12}$, and the size of the spatial window at this time is recorded as the optimal size of the first spatial window. Steps (iii) to (v) are repeated until the spatial window covers the main girder of the bridge.

(6) The optimal spatial window size is recorded for the first spatial window that was determined in Step (v).

(7) The lateral boundary of the spatial window is moved to the longitudinal bridge, and the initial size of the new spatial window is set, as shown in Figure 3.

(8) Steps (ii) to (vi) are repeated to determine the optimal size of the second spatial window.

(9) Steps (vii) to (viii) are repeated to complete the division of all spatial windows of the distributed strain of the bridge, as shown in Figure 4.

In different spatial windows, the correlation of the strain of measured points is different. Only the spatial window with a strong correlation of the measured points strain can be used to establish a strain correlation model with a good effect. Therefore, a clustering algorithm is adopted to obtain the spatial windows with a strong correlation of the measured points strain as the final retained spatial window. The specific steps are as follows:

(1) The size evaluation index of any two spatial windows are taken as the initial values of the size evaluation index mean values of the two types of spatial windows. The mean values of the size evaluation index of the spatial windows for the first category and the second category are denoted as χ_C^1 and χ_C^2, respectively.

(2) The distance between the size evaluation index of each spatial window and the mean value of the size evaluation index of the spatial window of the first category or the second category is calculated, as shown in the following equation:

$$\begin{aligned} \varsigma_{r1} &= \sqrt{\left(C_r - \chi_C^1\right)}, \\ \varsigma_{r2} &= \sqrt{\left(C_r - \chi_C^2\right)}, \end{aligned} \tag{17}$$

where C_r is the size evaluation index of the rth spatial window and ς_{r1} and ς_{r2} are the distances between the rth spatial window and the first or second category, respectively.

(3) If $\varsigma_{r1} < \varsigma_{r2}$, the rth spatial window is classified into the first category; otherwise, the rth spatial window is divided into the second category.

(4) Steps (ii) and (iii) are repeated to complete the classification of all spatial windows, and the mean values of the size evaluation indexes of the spatial windows of the first category and the second category are updated.

(5) Steps (ii) and (iv) are repeated until the mean values of the size evaluation indexes of the spatial windows of the first category and the second category are unchanged; then, the classification ends.

The spatial window with a larger mean value of the size evaluation index is taken as the final retained spatial window. Regarding those measured points that are not within the final retained spatial window, the strain monitoring data can be analyzed by using the traditional structural condition diagnosis method based on principal component analysis (as described in Section 4.2.4).

3. Cross-Diagnosis Algorithm for the Structural Condition of Long-Span Suspension Bridges Based on the Spatial Windows of Distributed Strain Data

3.1. Correlation Model of Distributed Strain Data for One Spatial Window. Due to the complex structure of the long-span suspension bridge, the strain data of the main girder structure have a strong nonlinear degree. Therefore, in this section, a deep neural network is used to construct the correlation model between the strain data of high-density measured points in one whole spatial window. Convolutional neural networks are among the most widely used algorithms in the field of deep learning. Many excellent results have been obtained in many practical applications in recent years by using this algorithm. Since the distributed strain data of the main girder structure at each moment are one-dimensional data, a one-dimensional convolutional neural network is used to construct the correlation model between the distributed strain data of the symmetric area in one whole spatial window.

The one-dimensional convolutional neural network is constructed by taking the structurally distributed strain monitoring data of the right area of the spatial window as input and the distributed strain monitoring data of the left area of the spatial window as output. The convolutional neural network needs to use multiple convolutional layers and pooling layers. The processing method of the convolutional layer is as follows:

$$J_{\mathrm{ij}}^{c1} = f^c\left(\sum_{o=0}^{N^C-1} U_{i(j+o)} w_o^{c1} + z_h^{c1}\right), \tag{18}$$

where $U_{i(j+o)}$ is the $(j+o)$-th input strain data at the ith time point, w_o^{c1} is the oth parameter of the convolution kernel $c1$, z_h^{c1} is the bias of the convolution kernel $c1$, N^C is the size of the convolution kernel $c1$, J_{ij}^{c1} is the output obtained from the jth to $(j+N^C-1)$-th input data processed by the convolution kernel $c1$, and $f^c(\cdot)$ is the activation function of the convolutional layer.

In this section, the ReLu function is used as the activation function of the convolutional layer [48], as shown in the following equation:

$$f^c(x) = \max(0, x). \tag{19}$$

The output data of the convolutional layer are further processed by the pooling layer to reduce the number of neurons in each layer. When the pooling layer is processed, the output data of the convolutional layer are divided into various intervals, and then the data of each interval are processed separately. The processing method of the data in the interval is shown in the following equation:

$$J_{\mathrm{ij}}^{s1} = \max\left(J_{\mathrm{ij},1}^{c1}, J_{\mathrm{ij},2}^{c1}, \ldots, J_{\mathrm{ij},n_s}^{c1}\right), \tag{20}$$

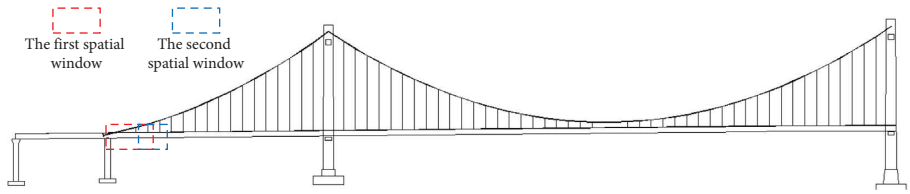

Figure 3: The location of the second spatial window.

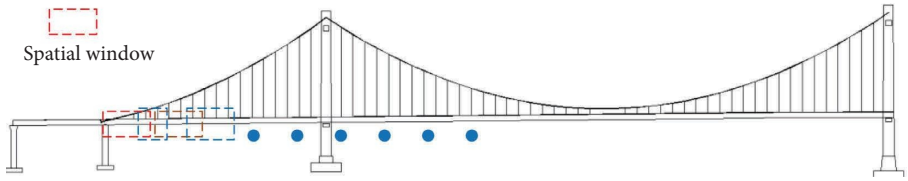

Figure 4: Locations of all spatial windows.

where J_{ij}^{s1} is the jth output of the pooling layer $s1$, J_{ij,n_s}^{c1} is the n_sth value of the interval, and n_s is the size of the interval corresponding to the jth output of the pooling layer $s1$.

After the input data are processed by multiple convolutional and pooling layers, they are connected to the output layer through a fully connected layer. Fully connected layers are processed in a similar way to convolutional layers, except that the fully connected layer uses a convolution kernel of the same size as the input, so that each input data of the fully connected layer only outputs one data through the convolution kernel.

Through the combination of multiple convolutional layers and pooling layers, the features of the distributed strain of the main girder structure can be extracted. Through the fully connected layer, the feature is connected to the output layer, and the whole one-dimensional convolutional neural network model is finally constructed. The structure of the one-dimensional convolutional neural network model is shown in Figure 5.

The correlation model of distributed strain in the spatial window constructed by the above one-dimensional convolutional neural network can be expressed as follows:

$$\widehat{\mathbf{U}}_i^r = f_{\mathrm{CNN1}}^r\left(\mathbf{P}_i^r\right), \tag{21}$$

where $\widehat{\mathbf{U}}_i^r$ is the predicted value of the distributed strain, $\mathbf{U}_i^r$ in the spatial window, and $f_{\mathrm{CNN1}}^r(\cdot)$ is the correlation model between the distributed strain monitoring data in the rth spatial window (its input is the strain monitoring data of the measured points in the right area, and its output is the strain monitoring data of the measured points in the left area).

3.2. Cross-Diagnosis Algorithm That Determines the Structural Conditions of Long-Span Suspension Bridges. The structural damage of long-span suspension bridges often occurs in local areas. If the abnormal data caused by the local damage are taken as the input or output of the correlation model of distributed strain data, the results of the model will inevitably be different. Based on this principle, a cross-diagnosis algorithm that determines the structural conditions of long-span suspension bridges is proposed.

Since the left and right areas of the spatial window are symmetric, a correlation model similar to that in equation (21) can be established, as shown in the following equation:

$$\widehat{\mathbf{P}}_i^r = f_{\mathrm{CNN2}}^r\left(\mathbf{U}_i^r\right), \tag{22}$$

where $\widehat{\mathbf{P}}_i^r$ is the predicted value of the distributed strain, $\mathbf{P}_i^r$ of the structure in the spatial window, and $f_{\mathrm{CNN2}}^r(\cdot)$ is the correlation model between the distributed strain monitoring data in the rth spatial window (its input is the strain monitoring data of the measured points in the left area, and its output is the strain monitoring data of the measured points in the right area).

Regarding the left area $\mathbf{U}^r$ and the right area $\mathbf{P}^r$ of the rth spatial window, at the ith time point, the residual of the correlation model of bridge structural strain in the left area $\mathbf{U}^r$ of the spatial window can be calculated by using the following equation:

$$\mathbf{e}_i = \mathbf{U}_i^r - \widehat{\mathbf{U}}_i^r = \mathbf{U}_i^r - f_{\mathrm{CNN1}}^r\left(\mathbf{P}_i^r\right) = \left[e_{i1,r}, e_{i2,r}, \ldots, e_{ij,r}, \ldots, e_{in,r}\right]^{\mathrm{T}}, \tag{23}$$

where $e_{ij,r}$ is the strain residual value of the jth measured point in the rth spatial window at the ith time point.

Since the size of the spatial window is generally large, the spatial windows of bridge structures can be divided into multiple areas that can be diagnosed to reflect the strain distribution characteristics of bridge structures with further accuracy. The strain residual of the areas to be diagnosed can be shown as follows:

$$\mathbf{e}_i = \mathbf{U}_i^r - \widehat{\mathbf{U}}_i^r = \left[\mathbf{e}_i^1, \mathbf{e}_i^2, \ldots, \mathbf{e}_i^v\right]^{\mathrm{T}}, \tag{24}$$

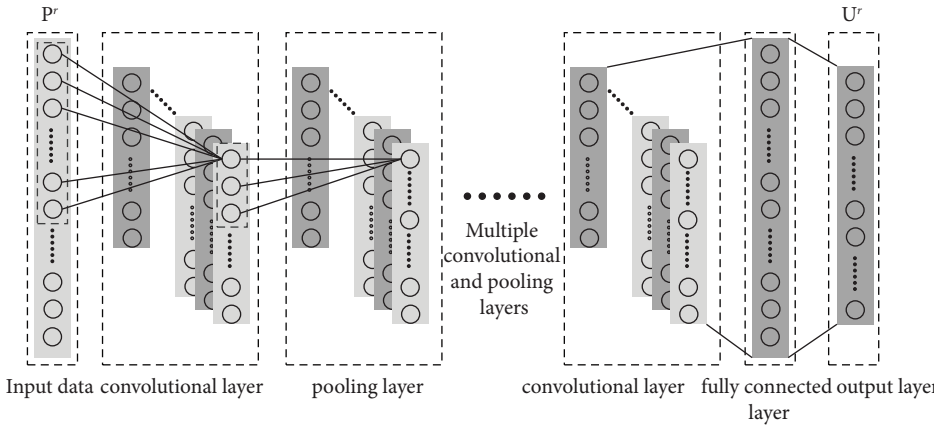

Figure 5: Sketch of the one-dimensional convolutional neural network.

where $\mathbf{e}_i^v$ is the strain residual vector of the v th area to be diagnosed at the ith time point.

By using equation (23), the strain residual matrix in the spatial window under the reference state (the bridge structure is in a healthy state) can be calculated, and the calculated result can be expressed as

$$\begin{aligned}\mathbf{e} &= \left[\mathbf{e}_1, \mathbf{e}_2, \ldots, \mathbf{e}_i, \ldots, \mathbf{e}_s\right] \\ &= \left[\mathbf{e}^1, \mathbf{e}^2, \ldots, \mathbf{e}^v\right]^{\mathrm{T}} \\ &= \begin{bmatrix} e_{11,r}^1 & e_{12,r}^1 & \cdots & e_{1s,r}^1 \\ e_{21,r}^1 & e_{22,r}^1 & & \\ \vdots & & \ddots & \vdots \\ e_{n1,r}^v & & \cdots & e_{ns,r}^v \end{bmatrix},\end{aligned} \tag{25}$$

where s is the total number of samples in the reference state; $\mathbf{e}^v$ is the strain residual matrix of the vth area to be diagnosed under the reference state; and $e_{ns,r}^v$ is the strain residual value of the nth measured point in the rth spatial window in the reference state at the sth time point, belonging to the vth area to be diagnosed.

Based on the Mahalanobis distance [49], the structural condition diagnosis index $\mathbf{Y}_v$ of each area that is diagnosed in the spatial window under the reference state can be calculated by using the following equation:

$$\mathbf{Y}_v = \mathrm{diag}\left(\left(\mathbf{e}^v - \boldsymbol{\mu}_{\mathbf{e}^v}\right)^{\mathrm{T}} \boldsymbol{\Sigma}_{\mathbf{e}^v\mathbf{e}^v}^{-1} \left(\mathbf{e}^v - \boldsymbol{\mu}_{\mathbf{e}^v}\right)\right)^{1/2}, \tag{26}$$

$$\boldsymbol{\Sigma}_{\mathbf{e}^v\mathbf{e}^v} = \frac{v}{n}\left(\mathbf{e}^v - \boldsymbol{\mu}_{\mathbf{e}^v}\right)\left(\mathbf{e}^v - \boldsymbol{\mu}_{\mathbf{e}^v}\right)^{\mathrm{T}}, \tag{27}$$

where $\boldsymbol{\mu}_{\mathbf{e}^v}$ is the mean value vector of $\mathbf{e}^v$, $\boldsymbol{\Sigma}_{\mathbf{e}^v\mathbf{e}^v}$ is the covariance matrix of $\mathbf{e}^v$, and $\mathrm{diag}(\cdot)$ denotes extraction of elements from the main diagonal of a matrix.

The structural condition diagnosis index in each area to be diagnosed is calculated according to the above equation. Then, the structural condition diagnosis index in the spatial window can be expressed as

$$\begin{aligned}\mathbf{Y} &= \left[\mathbf{Y}_1, \mathbf{Y}_2, \ldots, \mathbf{Y}_v\right]^{\mathrm{T}} \\ &= \begin{bmatrix} y_{11,r} & y_{12,r} & \cdots & y_{1s,r} \\ y_{21,r} & y_{22,r} & & \\ \vdots & & \ddots & \vdots \\ y_{v1,r} & & \cdots & y_{vs,r} \end{bmatrix},\end{aligned} \tag{28}$$

where $y_{vs,r}$ is the structural condition diagnosis index of the vth area to be diagnosed of the rth spatial window at the sth time point.

The structural condition diagnosis indexes of each area are rearranged to be diagnosed in matrix Y from the smallest to the largest, and the following matrix can be obtained as follows:

$$\mathbf{Y} = \begin{bmatrix} y_{1,r}^1 & y_{1,r}^2 & \cdots & y_{1,r}^s \\ y_{2,r}^1 & y_{2,r}^2 & & \\ \vdots & & \ddots & \vdots \\ y_{v,r}^1 & & \cdots & y_{v,r}^s \end{bmatrix}, \tag{29}$$

where $y_{v,r}^s$ is the sth value in the sequence of the structural condition diagnosis index arranged from small to large in the vth area to be diagnosed in the rth spatial window.

The threshold of the condition of a bridge structure can be calculated by the following equation:

$$\begin{aligned}\mathbf{T}_y &= \left(y_{1,r}^{0.95s}, y_{2,r}^{0.95s}, \ldots, y_{v,r}^{0.95s}\right)^{\mathrm{T}} \\ &= \left(\mathrm{TY}_1, \mathrm{TY}_2, \ldots, \mathrm{TY}_v\right)^{\mathrm{T}},\end{aligned} \tag{30}$$

where TY_v is the threshold of the bridge structure state of the vth area to be diagnosed.

The strain residual of the spatial window in the state to be diagnosed can be expressed as

$$\mathbf{e}' = \left(\mathbf{e}_1', \mathbf{e}_2', \ldots, \mathbf{e}_i', \ldots, \mathbf{e}_g'\right) = \left(\mathbf{e}^{1'}, \mathbf{e}^{2'}, \ldots, \mathbf{e}^{v'}\right)^{\mathrm{T}}, \tag{31}$$

where g is the total number of samples in the state to be diagnosed.

In the state to be diagnosed, the structural condition diagnosis index in the vth area in the spatial window can be calculated according to the following equation:

$$\mathbf{Y}_v' = \operatorname{diag}\left(\left(\mathbf{e}^{v'} - \boldsymbol{\mu}_{\mathbf{e}^{v'}}\right)^{\mathrm{T}} \boldsymbol{\Sigma}_{\mathbf{e}^v\mathbf{e}^v}^{-1}\left(\mathbf{e}^{v'} - \boldsymbol{\mu}_{\mathbf{e}^{v'}}\right)\right)^{1/2}, \tag{32}$$

where $\boldsymbol{\mu}_{\mathbf{e}^{v'}}$ is the mean value vector of $\mathbf{e}^{v'}$.

The state diagnosis index of the bridge in the state to be diagnosed $\mathbf{Y}'$ can be expressed as follows:

$$\mathbf{Y}' = \begin{bmatrix} y_{11,r}' & y_{12,r}' & \cdots & y_{1g,r}' \\ y_{21,r}' & y_{22,r}' & & \\ \vdots & & \ddots & \vdots \\ y_{v1,r}' & & \cdots & y_{vg,r}' \end{bmatrix}. \tag{33}$$

The above structural condition diagnosis index of the bridge is obtained based on the residual of the correlation model of distributed strain data calculated by using equation (23). The correlation model used for this residual is obtained by taking the structural strain monitoring data of the right area in the spatial window as input and the structural distributed strain of the left area as output. Based on equation (22) and by taking the monitoring data of structural strain in the right area of the spatial window as the output and the distributed structural strain in the left area as the input, the residual as shown in the following equation can be obtained as follows:

$$\mathbf{e}_{\mathrm{UP}} = \mathbf{P}^r - \widehat{\mathbf{P}}^r = \mathbf{P}^r - f_{\mathrm{CNN2}}^r\left(\mathbf{U}_i^r\right). \tag{34}$$

According to equations (23) to (33), the bridge structural condition diagnosis index and the threshold calculated by using $\mathbf{e}_{\mathrm{UP}}$ under the state to be diagnosed are shown in the following equation:

$$\mathbf{R}' = \begin{bmatrix} R_{11,r}' & R_{12,r}' & \cdots & R_{1g,r}' \\ R_{21,r}' & R_{22,r}' & & \\ \vdots & & \ddots & \vdots \\ R_{v1,r}' & & \cdots & R_{vg,r}' \end{bmatrix}, \tag{35}$$

$$\mathbf{T}_{\mathrm{R}} = \left(\mathrm{TR}_1, \mathrm{TR}_2, \ldots \mathrm{TR}_v\right)^{\mathrm{T}}, \tag{36}$$

where $R_{vg,r}'$ is the bridge structural condition diagnosis index of the vth area in the right area of the rth spatial window under the state to be diagnosed at the gth time point, and TR_v is the threshold of the vth area in the right area of the rth spatial window.

Under the state to be diagnosed, when the structural condition diagnosis index of the bridge exceeds the corresponding threshold, the bridge structure is determined to be damaged. On this basis, the cross-diagnosis method is further used to locate the area where the strain anomaly is located.

Structural damage is often localized. When the strain data of measured points in the damaged area are used as the input of the correlation model, the abnormality of local measured points as the input has little influence on the output results due to the large number of measured points in the spatial window. Therefore, in the above cases, the output is basically normal. When the strain data of the measured point in the damaged area are used as the output of the spatial correlation model, the output result will only be abnormal near the damaged area since the input is still in a normal state.

If damage occurs in Area U as shown in Figure 1, the structural strain monitoring data in Area U are used to predict the structural strain of Area P by using the correlation model, and the structural condition diagnosis index of the bridge will not exceed the threshold. At the same time, when the structural strain monitoring data in Area P are used to predict the structural strain in Area U, the structural condition diagnosis index of some measured points exceeds the threshold value.

According to the above analysis, after obtaining the bridge structural condition diagnosis index in the symmetric area of the spatial window by using equations (23) to (36), the damage region can be determined by the following steps.

(1) Whether the bridge structural condition diagnosis indexes in Area U and Area P are over the limit can be determined by using equation (37) and (38), respectively:

$$R_{vg,r}' > \mathrm{TR}_v, \tag{37}$$

$$y_{vg,r}' > \mathrm{TY}_v. \tag{38}$$

(2) If equation (37) is valid, the bridge structural condition diagnosis index in the vth region to the right of Area P can be determined to be beyond the limit. If equation (38) is valid, the bridge structural condition diagnosis index in the vth region to the left of Area U can be determined to be over the limit.

(3) If all the bridge structural condition diagnosis indexes corresponding to the region to be diagnosed in Area U do not exceed the limit and there are several bridge structural condition diagnosis indexes corresponding to the region to be diagnosed in Area P that exceed the limit, then the strain abnormal area can be determined to be Area P.

(4) If all the bridge structural condition diagnosis indexes corresponding to the region to be diagnosed in Area P do not exceed the limit and there are several bridge structural condition diagnosis indexes corresponding to the region to be diagnosed in Area $\boldsymbol{U}$ that exceed the limit, then the strain abnormal area can be determined to be Area U.

A flowchart of the proposed method is presented in Figure 6.

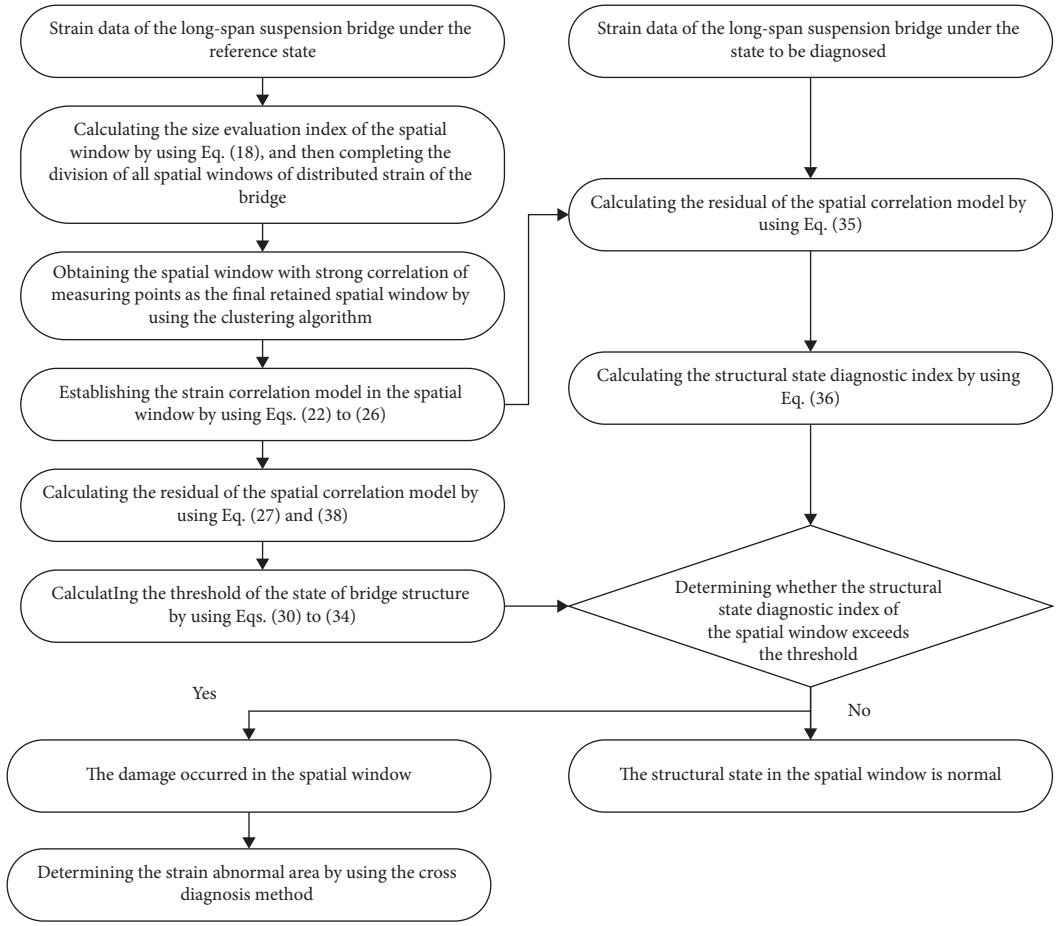

Figure 6: Flowchart of the proposed method.

4. Case Study Verification

4.1. Introduction to the Yellow River Fenghuang Bridge. The engineering example used in this section is the main bridge of the Yellow River Fenghuang Bridge in Jinan, China. The bridge is a three-tower, self-anchored suspension bridge and is an important passage across the Yellow River. Its span layout is (70 m + 168 m + 428 m + 428 m + 168 m + 70 m). The bridge deck is a steel-concrete composite structure, and the bored pile foundation is used as the substructure. A photo of the bridge is shown in Figure 7.

4.2. Numerical Case Study

4.2.1. Finite Element Model of the Yellow River Fenghuang Bridge. By using the design data of the Yellow River Fenghuang Bridge, the finite element model of the bridge structure was established by using the finite element software ANSYS. Beam188 elements were used to simulate the main girder, and link10 elements were used to simulate the boom and main cable. The finite element model is shown in Figure 8.

The main girder section of the finite element model of the bridge is shown in Figure 9.

A random vehicle load was applied on the bridge by means of nodal forces. The load value of the node under each time point was randomly selected according to the uniform probability distribution. The probability density function of vehicle loads is as follows [50]:

$$f(x) = \frac{1}{x\sqrt{2\pi}\beta}\exp\left(\frac{-(\ln x - \alpha)^2}{2\beta^2}\right), \quad (39)$$

where x is the vehicle weight load with units of kN; α is the distribution parameter, and is 2.57; β is the distribution parameter, and is 0.8485; and $\exp(\cdot)$ is the exponential function based on the natural constant.

Ignoring daily temperature variation, a periodic function was used to simulate annual temperature variation, and a total of 12,000 temperature data points were simulated, as shown in Figure 10.

A random vehicle load as shown in equation (39) was applied to each node of the finite element model. Simultaneously, the corresponding temperature shown in Figure 10 was applied at each time point to obtain the bridge structure strain data at 12,000 time points. The measured points at and near the midspan of the bridge are selected as the key measured points, as shown in Figure 11. The strain data of key measured points are shown in Figure 12.

Figure 7: Photo of the Yellow River Fenghuang Bridge.

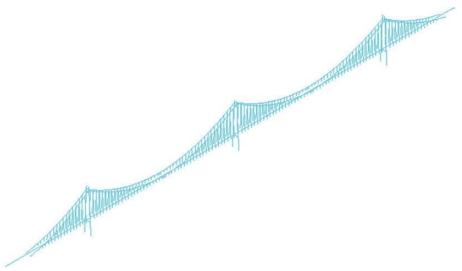

Figure 8: Finite element model of the bridge.

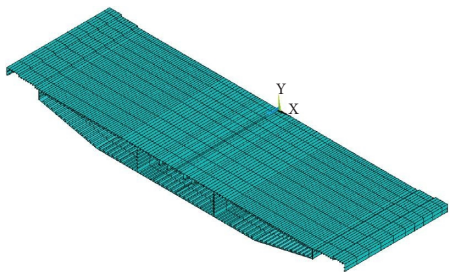

Figure 9: Main girder section of the finite element model of the bridge.

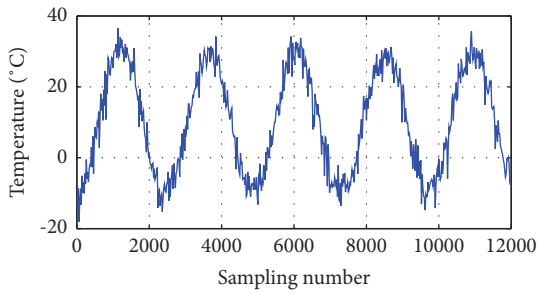

Figure 10: Temperature change regulation of the simulated air environment.

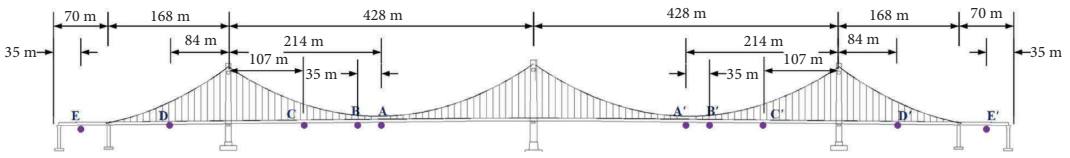

Figure 11: Key measured points of the bridge.

The temperature-induced strain belongs to the low-frequency part of strain data and the traffic-induced strain belongs to the high-frequency the part of strain data [51, 52]. Therefore, in order to analyze temperature-induced and traffic-induced structural strains, a curve fitting method is used to process the original data, and the fitted curve can approximately be regarded as the temperature-induced strain. The traffic-induced strain can be obtained by

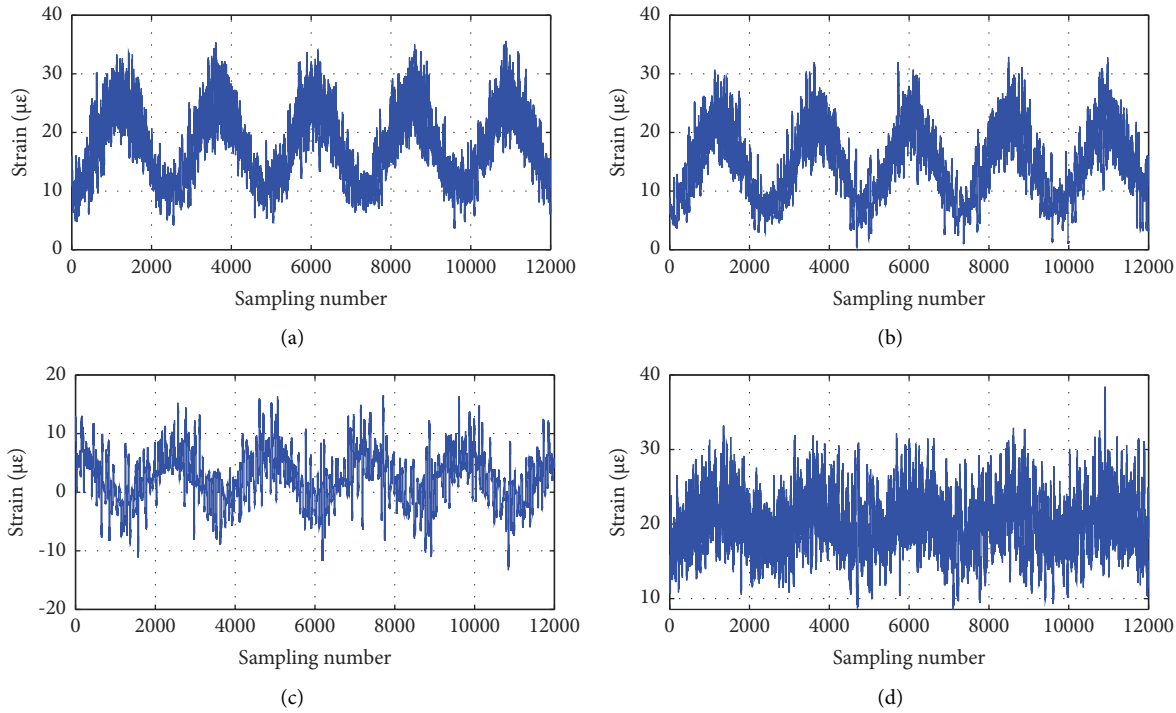

Figure 12: Strain data of key measured points. (a) Key measured point *A*. (b) Key measured point *B*. (c) Key measured point *C*. (d) Key measured point *D*.

subtracting the temperature-induced strain from the original strain, as shown in Figure 13. It can be seen from Figure 13 that the temperature-induced strain data of the two measured points are relatively similar. This phenomenon indicates that the strain data of the symmetrical measured points of the bridge have a certain correlation under the effect of long-term temperature, and this is consistent with equation (2). In contrast to the temperature-induced strain data, the traffic-induced strain data of the symmetrical measured points are random and have no obvious correlation.

In this paper, the structural damage of the main girder is simulated by reducing the elastic modulus of the materials. The specific methods are as follows: the structural condition of the bridge from the 1st to the 10000th time point is set as the healthy state, and the structural condition of the bridge from the 10001th to the 12000th time point is set as the damaged state. The elastic modulus at the simulated damage position of the bridge structure under the damaged state gradually changes linearly over time and reaches the minimum value at the 12000th time point. Detailed descriptions of the different cases are listed in Table 1.

4.2.2. Division of the Spatial Window of Distributed Strain Data. Using the method described in Section 2, the locations and classification results of all spatial windows obtained are shown in Figure 14.

Obviously, the evaluation index of the second type of space window is larger, so the second type of space window is retained. Since many measured points are in multiple different spatial windows, the spatial window in which the interior measured point is completely contained by other spatial windows is removed, and adjacent spatial windows with overlapping areas are merged. The final retained spatial windows are shown in Figure 15.

4.2.3. Diagnosis Results of the Structural Condition of the Bridge. The method described in Section 3 is adopted to establish the correlation model of the bridge structure distributed strain data with the data from the 1st to 10000th time points as the sample set. The strain residual of the model at the key point of the bridge in a healthy state is shown in Figure 16.

It can be seen from Figure 16 that the residual of the correlation model of the bridge structure distributed strain data is small and changes smoothly. This phenomenon indicates that this model can effectively reduce the influence of ambient temperature on the strain response of bridge structures.

Based on the two strain correlation models for estimating the strain data of the left region by using the strain data of the right region in the spatial window and estimating the strain data of the right region by using the strain data of the left region in the spatial window, the method described in Section 3 was adopted to diagnose the structural condition of the bridge. When the noise level of the monitoring data is 5%, the diagnosis results are shown in Figures 17 and 18.

It can be seen from Figures 17 and 18 that based on the strain correlation model that estimates the strain data of the left region by using the strain data of the right region in the spatial window, the bridge structural condition diagnosis

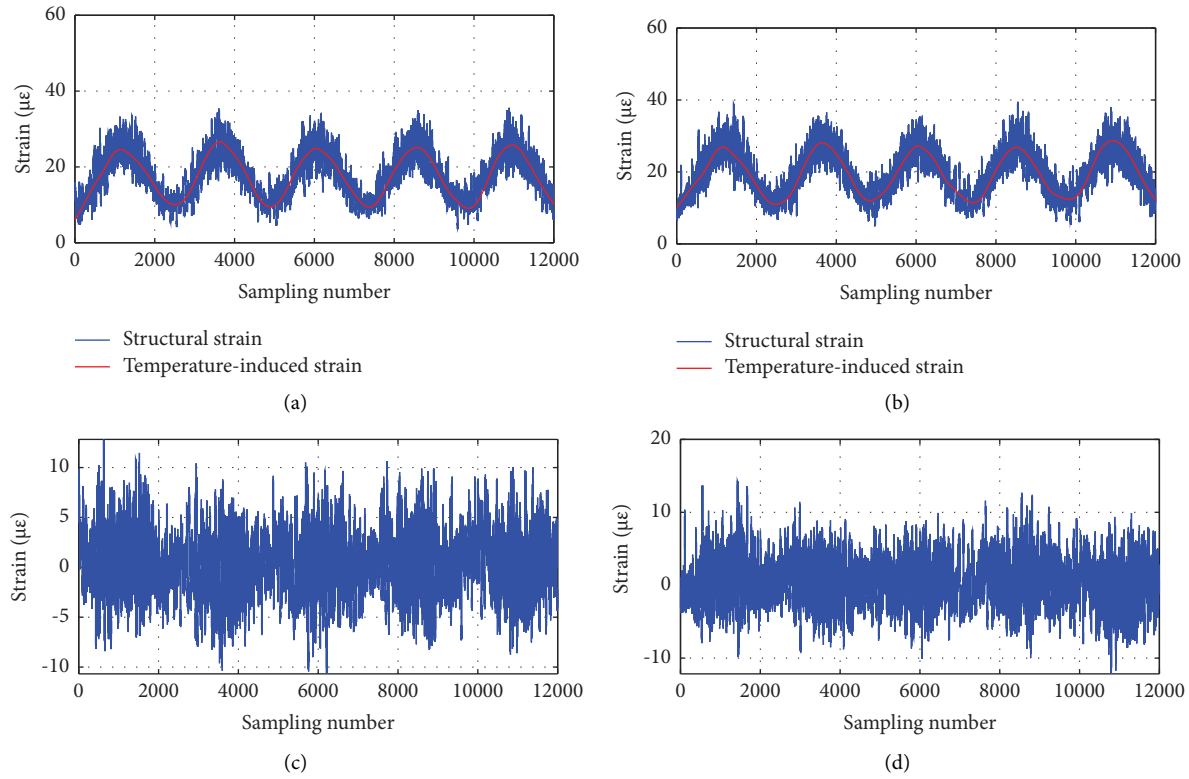

Figure 13: Temperature-induced and traffic-induced structural strains. (a) Temperature-induced strain at key measured point A. (b) Temperature-induced strain at key measured point A'. (c) Traffic-induced strain at key measured point A. (d) Traffic-induced strain at key measured point A'.

Table 1: Descriptions of the different cases.

Number	Description of case		
	Maximum damage extent (%)	Noise level (%)	Damaged region
Case 1	5.0	5.0	Key measured point A
Case 2	5.0	10.0	Key measured point A
Case 3	5.0	15.0	Key measured point A
Case 4	10.0	5.0	Key measured point A
Case 5	10.0	10.0	Key measured point A
Case 6	10.0	15.0	Key measured point A
Case 7	15.0	5.0	Key measured point A
Case 8	15.0	10.0	Key measured point A
Case 9	15.0	15.0	Key measured point A

index can be used to effectively diagnose the damage at Point A (even when the maximum damage extent is 5%), and the diagnosis indexes at other points are less than the threshold. Based on the strain correlation model for estimating the strain data of the right region by using the strain data of the left region in the spatial window, the bridge structural condition diagnosis index does not exceed the threshold at Point B and Point A. The above phenomenon is consistent with the conclusion in Section 3.

When the maximum damage extent is 5% and the noise level is also 5%, the summary diagnosis results of the bridge structure are shown in Figures 19 and 20.

As shown in Figures 19 and 20, it can be clearly determined that damage has occurred to the bridge structure, and the abnormal strain area is at the position of Point A. The results show that the proposed method can effectively diagnose the minor damage in the local area of the main girder and accurately determine the abnormal strain area.

To further analyze the ability of the proposed method to resist noise, simulated noise was added to the simulated data at a 10% damage extent, and the bridge structural condition diagnosis index at 10% and 15% noise degrees was obtained. The structural condition diagnosis index of the bridge at Points A and B is shown in Figure 21.

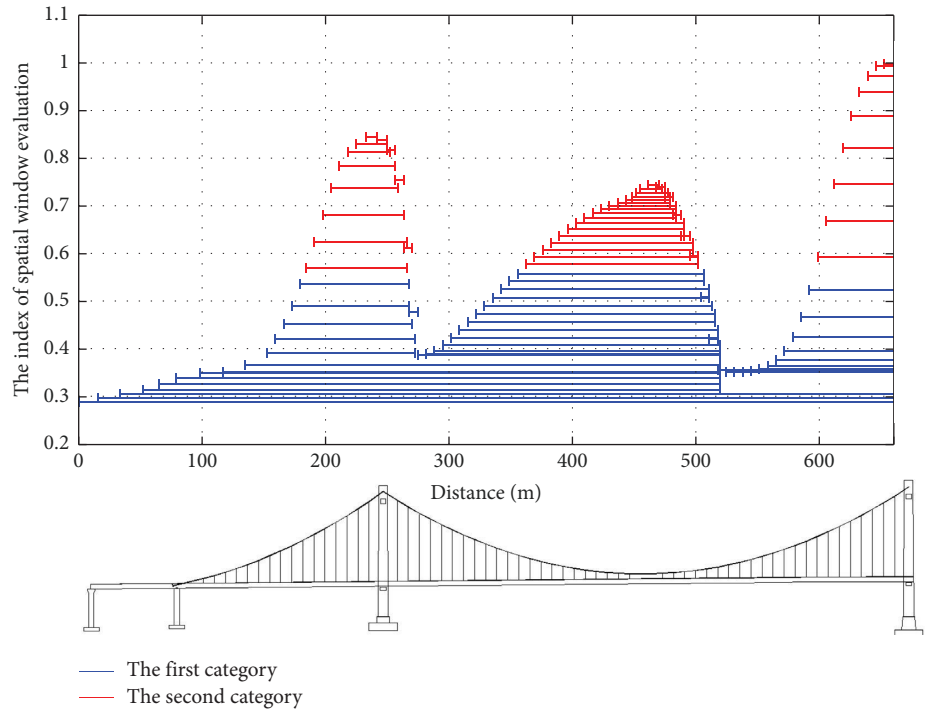

Figure 14: Locations and classification results of all spatial windows.

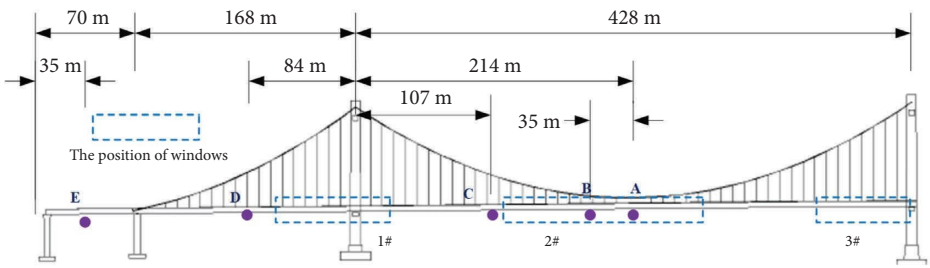

Figure 15: Final retained spatial windows.

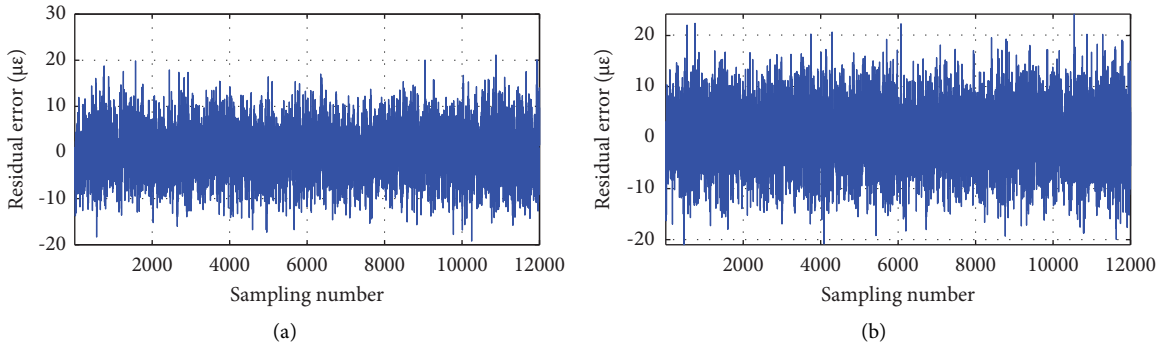

Figure 16: Residual of the strain correlation model at the key point. (a) Key measured point *A*. (b) Key measured point *B*.

As shown in Figure 21, the proposed method has a good antinoise interference ability when the damage extent is 10%. At a noise level of 15%, the structural condition diagnosis index of the bridge at Point *A* exceeds the threshold; that is, this method can identify the damage extent of 10% of the bridge structure at a noise level of 15%.

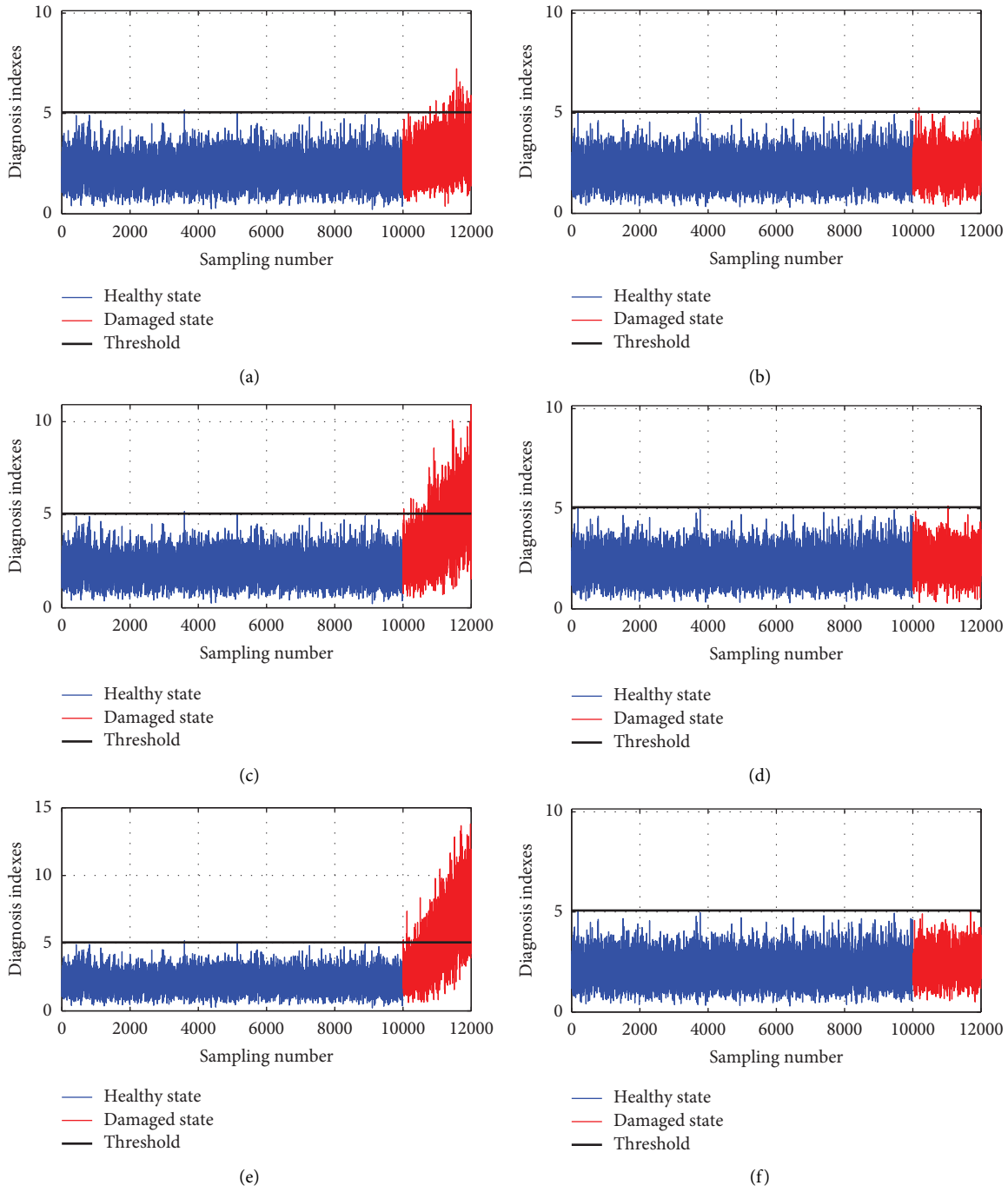

Figure 17: Results of the condition diagnosis of the bridge structure at the 5% noise level (based on the strain correlation model for estimating the strain data of the left region by using the strain data of the right region in the spatial window). (a) Key measured point *A* (maximum damage extent is 5%). (b) Key measured point *B* (maximum damage extent is 5%). (c) Key measured point *A* (maximum damage extent is 10%). (d) Key measured point *B* (maximum damage extent is 10%). (e) Key measured point *A* (maximum damage extent is 15%). (f) Key measured point *B* (maximum damage extent is 15%).

4.2.4. Performance Comparison of the Proposed Method with Other Methods. The proposed method is compared with the method based on principal component analysis (PCA) and the method based on a correlation model without a spatial window. In the method based on PCA, PCA is used to remove the environmental influence components, and then the Mahalanobis distance is used to calculate the corresponding diagnosis indexes of bridge structural conditions. The main difference between the method based on PCA and the proposed method is that it does not use the symmetric interval of the long-span bridge structure to establish the correlation model. The steps of the method based on PCA are described below.

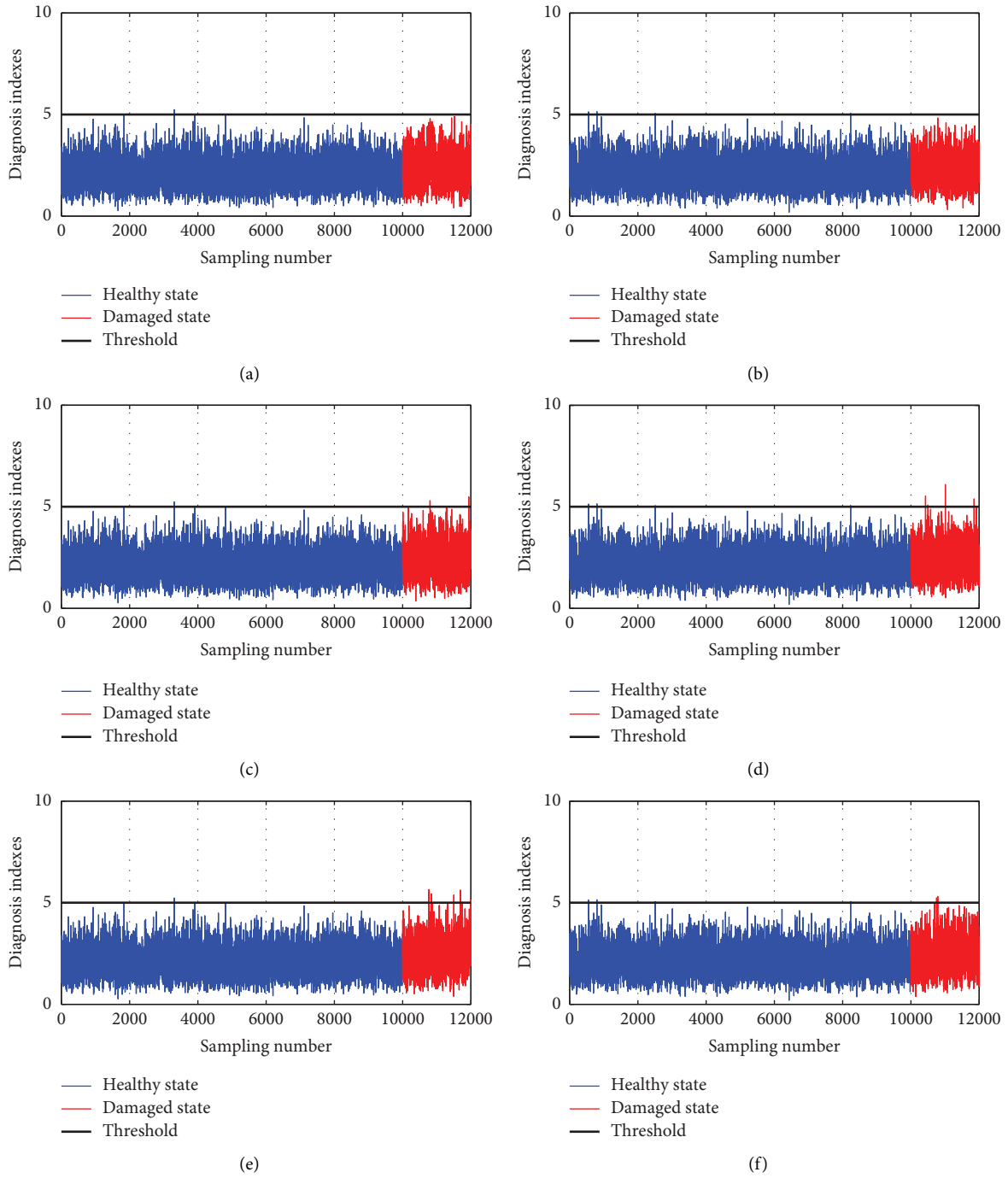

FIGURE 18: Results of the condition diagnosis of the bridge structure at the 5% noise level (based on the strain correlation model for estimating the strain data of the right region by using the strain data of the left region in the spatial window). (a) Key measured point A (maximum damage extent is 5%). (b) Key measured point B (maximum damage extent is 5%). (c) Key measured point A (maximum damage extent is 10%). (d) Key measured point B (maximum damage extent is 10%). (e) Key measured point A (maximum damage extent is 15%). (f) Key measured point B (maximum damage extent is 15%).

At the ith time point, the strain of the measured point in the region to be diagnosed can be expressed as follows:

$$\mathbf{U}_i = \left[U_{i1}, U_{i2}, \ldots, U_{ij}, \ldots\right]^{\mathrm{T}}, \tag{40}$$

where U_{ij} is the strain of the jth measured point at the ith time point.

The strain matrix of the region to be diagnosed at multiple time points can be expressed as

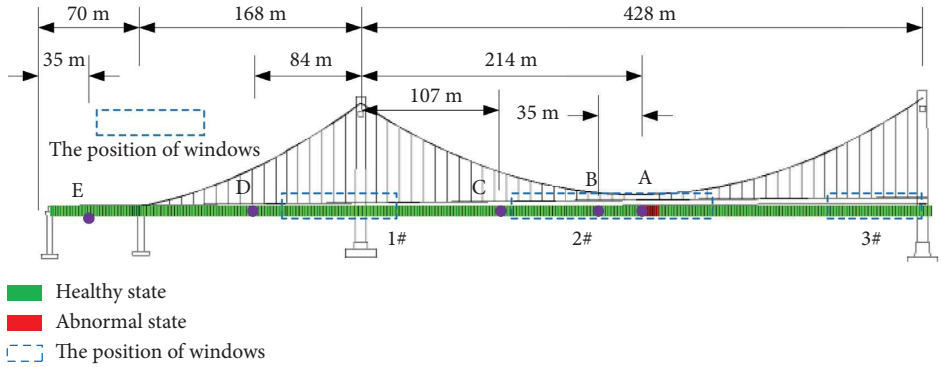

FIGURE 19: Summary diagnosis results of the bridge structure (case 1, based on the strain correlation model that estimates the strain data of the left region by using the strain data of the right region in the spatial window).

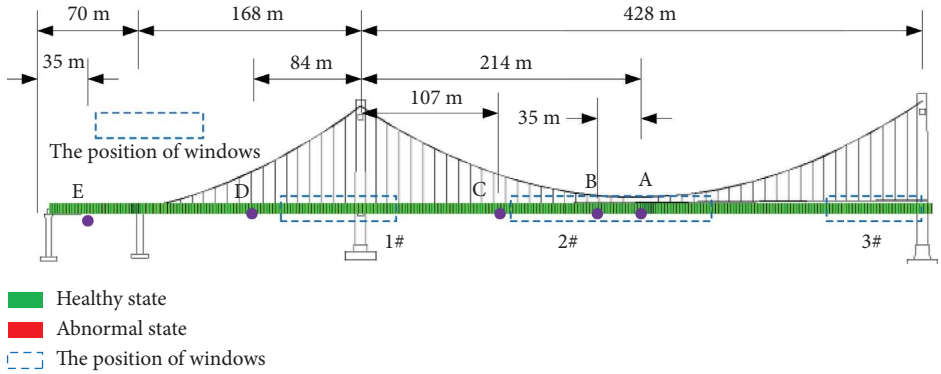

FIGURE 20: Summary diagnosis results of the bridge structure (case 1, based on the strain correlation model that estimates the strain data of the right region by using the strain data of the left region in the spatial window).

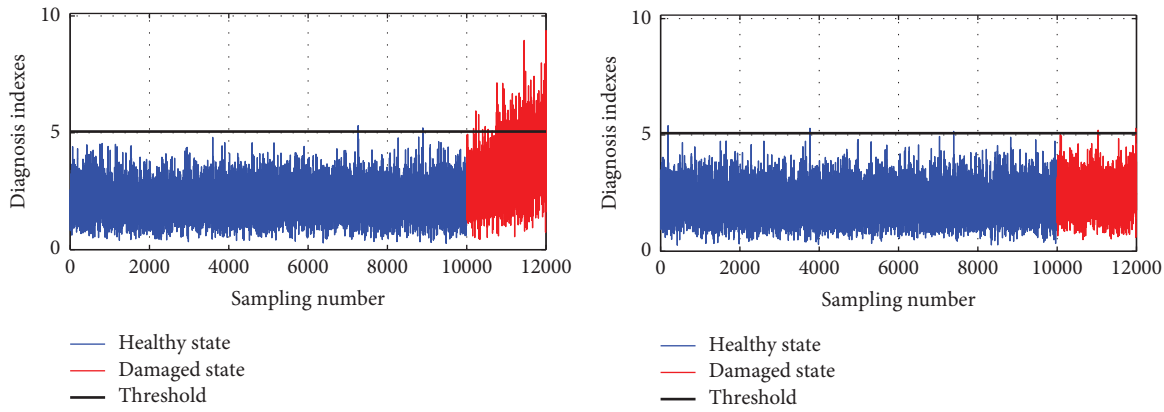

FIGURE 21: Continued.

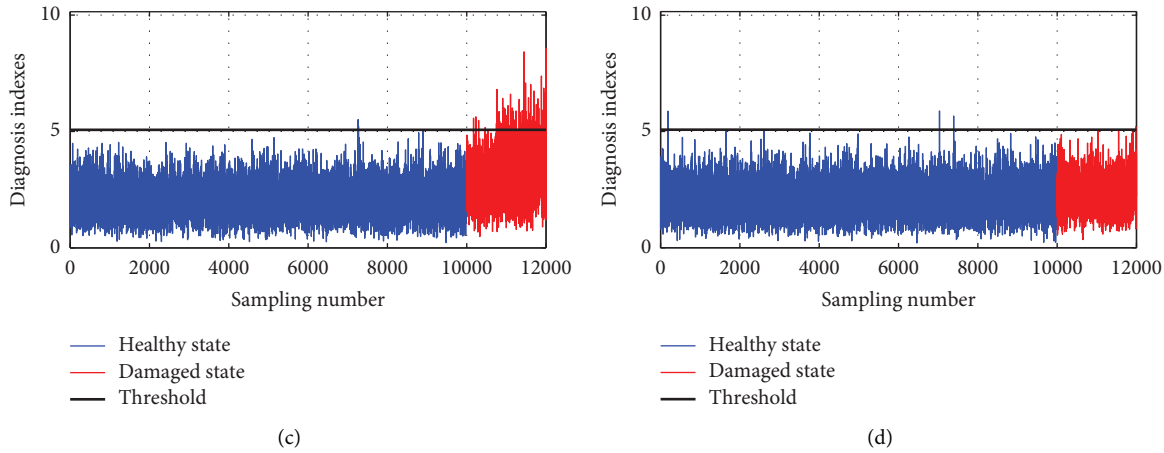

FIGURE 21: Results of the condition diagnosis of the bridge structure at 10% and 15% noise levels (based on the strain correlation model that estimates the strain data of the left region by using the strain data of the right region in the spatial window). (a) Key measured point A (the noise degree is 10%). (b) Key measured point B (the noise degree is 10%). (c) Key measured point A (the noise degree is 15%). (d) Key measured point B (the noise degree is 15%).

$$\mathbf{U} = \left[\mathbf{U}_1, \mathbf{U}_2, \ldots, \mathbf{U}_i, \ldots, \mathbf{U}_{n_u}\right], \tag{41}$$

where n_u is the total number of points contained.

The covariance matrix of $\mathbf{U}$ is constructed after centralized processing, and an eigenvalue decomposition of the covariance matrix is conducted, as shown in the following equation:

$$\frac{1}{n_u}\left(\mathbf{U} - \boldsymbol{\mu}_U\right)\left(\mathbf{U} - \boldsymbol{\mu}_U\right)^{\mathrm{T}} = \mathbf{ABA}^{\mathrm{T}}, \tag{42}$$

where $\boldsymbol{\mu}_U$ is the mean value vector of $\mathbf{U}$, and $\mathbf{B}$ is the eigenvalue matrix of $\mathbf{U}$.

$\mathbf{B}$ can be divided into two parts according to the size of the eigenvalue, as shown in the following equation:

$$\mathbf{B} = \begin{bmatrix} \mathbf{B}_1 & \mathbf{0} \\ \mathbf{0} & \mathbf{B}_2 \end{bmatrix}, \tag{43}$$

$\mathbf{B}_1$, which contains larger eigenvalues, is removed, and the part of the matrix $\mathbf{A}$ corresponding to $\mathbf{B}_2$, which is denoted as $\mathbf{A}_2$, is taken. The damage diagnostic feature that removes the environmental impact component can be expressed as

$$\mathbf{e}_u = \mathbf{A}_2^{\mathrm{T}}\left(\mathbf{U} - \boldsymbol{\mu}_U\right). \tag{44}$$

By substituting equation (44) into equation (26), the bridge structural condition diagnosis index based on PCA can be calculated to achieve bridge structural condition diagnosis.

In the method based on the correlation model without a spatial window, all the other processes are the same as those of the proposed method except that the spatial window is not divided and the strain data of the half-bridge are taken as the input and output of the correlation model. The bridge structure state diagnosis results of the method based on PCA, the method based on the correlation model without a spatial window, and the proposed method are shown in Figure 22.

It can be seen from Figure 22 that, compared with the proposed method, the diagnostic accuracy of the method based on the correlation model without a spatial window and the method based on PCA is lower, and it is difficult to identify the damage at the 5% noise level and 10% damage extent.

4.3. Case Study of the Real Bridge

4.3.1. Introduction of the SHM System of the Real Bridge. Distributed optical fiber sensors were installed in the steel box girder of the Yellow River Fenghuang Bridge main bridge. The distributed optical fiber sensing technology based on Brillouin scattering was used to obtain the strain monitoring data of the steel box girder with a spatial resolution of 20 cm. The layout diagram of the distributed optical fiber sensors is shown in Figure 23.

The distributed optical fiber sensor is connected to the steel box girder through the all-paste method, and the strain monitoring data of the bridge were collected in December 2021, as shown in Figure 24.

It can be seen from Figures 24(b) and 24(d) that the strain data of measured points A and A' contain the part of periodic changes caused by environmental temperature and other parts caused by various loads such as vehicles, and this is consistent with equation (1). At the same time, it can be seen that the periodic changes in the strain data of the measured points A and A' are similar, showing that there is a correlation between the part of the strain caused by environmental temperature at the two measured points, and this is consistent with equation (2). Figure 24(e) further shows the correlation between the strain data of the two measured points, and it shows that there is indeed a correlation between the strain data of the symmetrical measured points of the bridge, which is consistent with equation (4) and provides a basis for the further diagnosis of the structural condition of long-span suspension bridges.

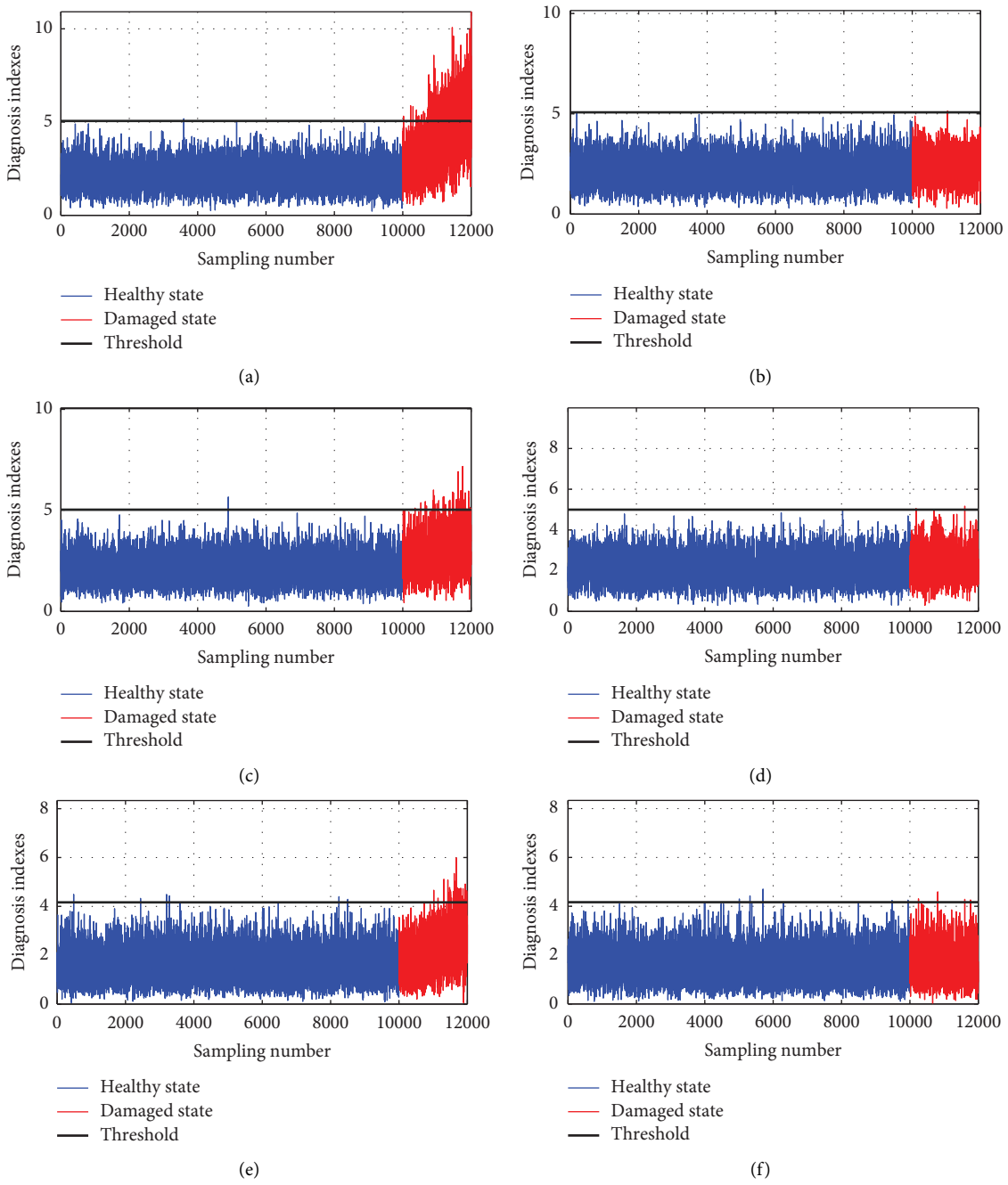

FIGURE 22: Results of the condition diagnosis of the bridge structure at a 5% noise level and 10% damage extent obtained by using the proposed method and other methods. (a) Key measured point *A* (the proposed method). (b) Key measured point *B* (the proposed method). (c) Key measured point *A* (the method based on the correlation model without a spatial window). (d) Key measured point *B* (the method based on the correlation model without a spatial window). (e) Key measured point *A* (the method based on PCA). (f) Key measured point *B* (the method based on PCA).

4.3.2. Division of the Spatial Window of Distributed Strain Data of the Real Bridge. Using the method described in Section 2, the locations and classification results of all spatial windows of the real bridge are obtained and shown in Figure 25.

Obviously, the evaluation index of the second type of space window is larger, so the second type of spatial window is retained. In accordance with the method in Section 4.2.2., the spatial window in which the interior measured point is completely contained by other spatial windows is removed, and adjacent spatial windows with overlapping areas are merged. The final retained spatial windows are shown in Figure 26. The spatial window obtained from the measured data is different from the results of the finite element, and the main difference is that the spatial window obtained from the measured data contains more main girder areas. The reason

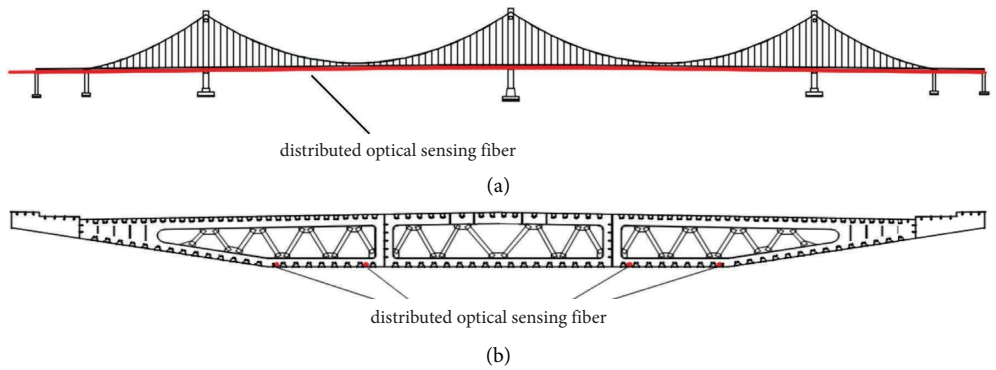

FIGURE 23: Sketch of the arrangement of the distributed optical sensing fiber. (a) Elevation layout diagram. (b) Cross-section layout diagram.

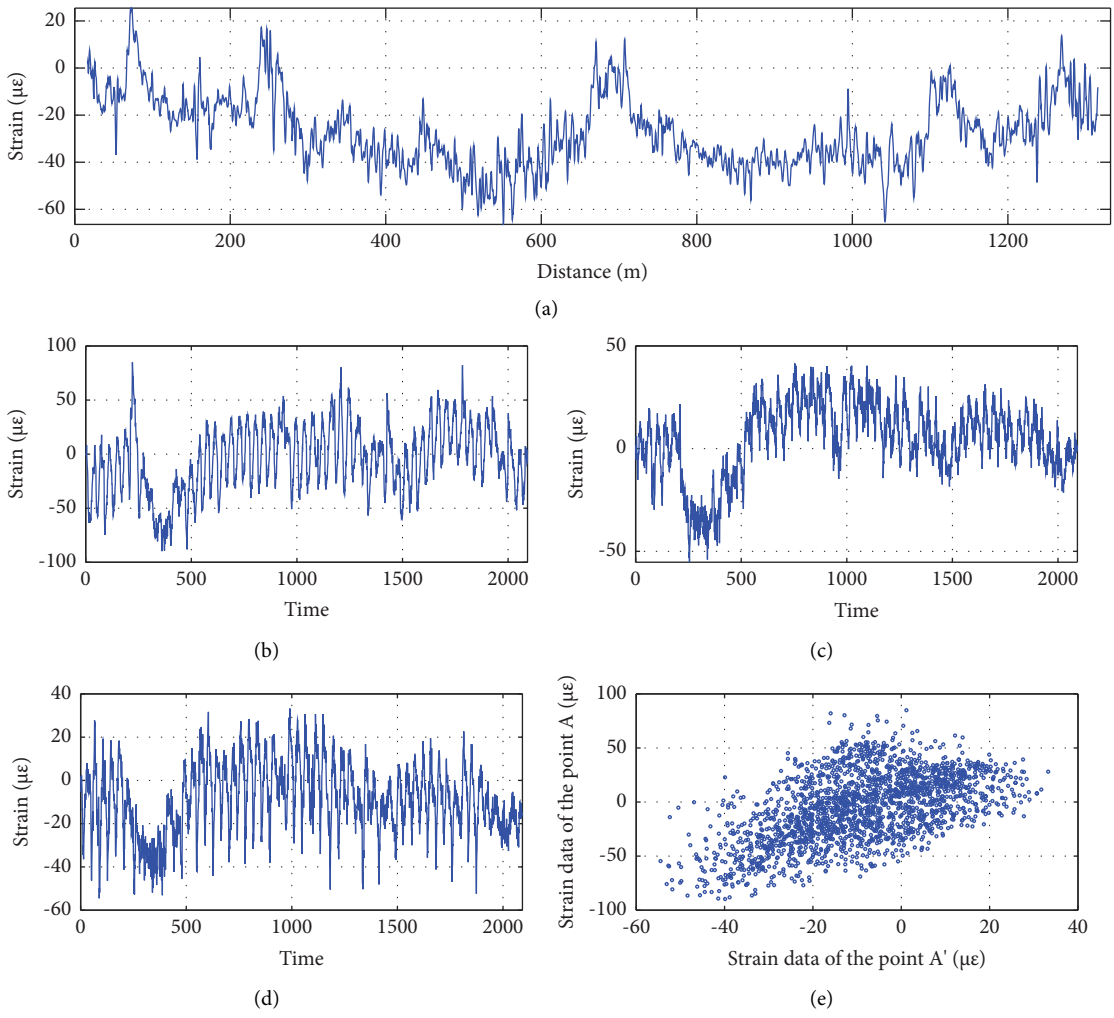

FIGURE 24: Strain monitoring data of the bridge. (a) Spatial distribution of the strain. (b) Strain data (point A). (c) Strain data (point B). (d) Strain data (point A'). (e) The correlation between strain data at point A and point A'.

for this phenomenon is perhaps that the influence of ambient temperature on the strain of the main girder varies with different vehicle and wind loads, leading to the difference in the correlation of the strain of the main girder.

4.3.3. Diagnosis Results of the Structural Condition of the Real Bridge. The method described in Section 3 is adopted to establish the correlation model of the distributed strain data of the real bridge with the data from the 1st to 1600th time

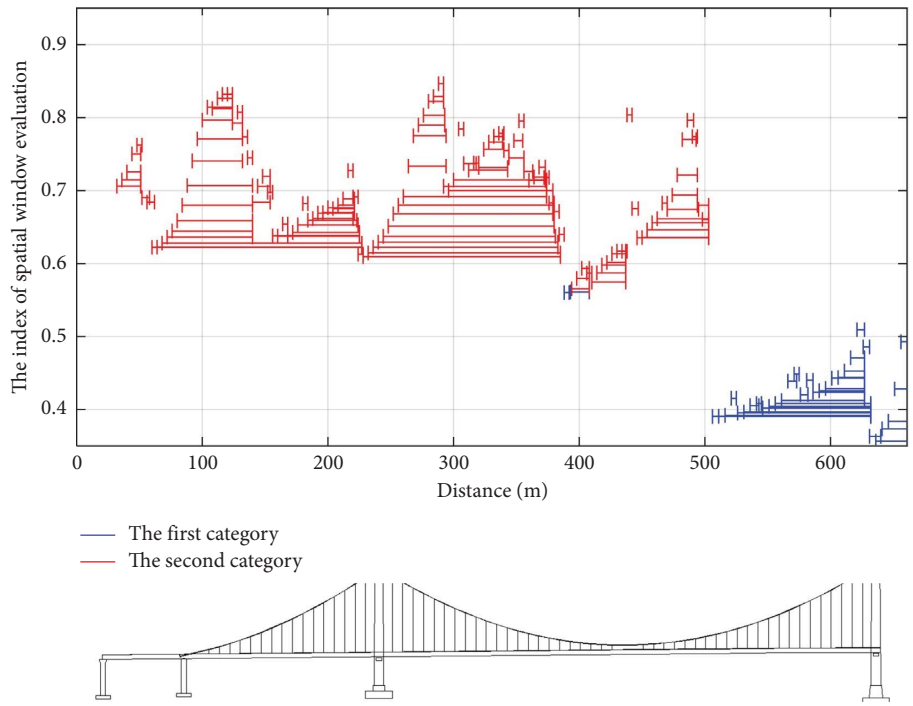

Figure 25: Locations and classification results of all spatial windows of the real bridge.

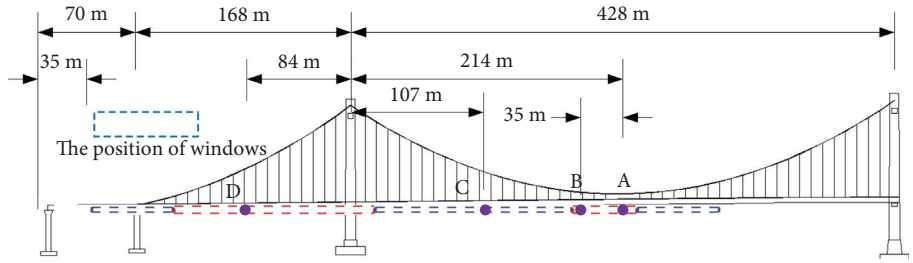

Figure 26: Final retained spatial windows of the real bridge.

points as the sample set. The strain residuals of the model at the key point of the bridge are shown in Figure 27.

It can be seen from Figure 27 that the residuals of the strain correlation model are small and change steadily, indicating that the proposed correlation model of the distributed strain data is effective. Based on the correlation model of distributed strain data, the diagnosis results of the proposed method are shown in Figure 28.

It can be seen from Figure 28 that, except for the accidental errors of some data, the structural condition diagnosis index of the bridge did not exceed the threshold and changed steadily, indicating that the bridge was in a healthy state. Since the bridge is a newly built bridge, it can be considered that no damage occurs, and this is consistent with the diagnosis results of the proposed method. The above results validate the effectiveness of the proposed method from the perspective of avoiding misdiagnosis.

To further verify the effectiveness of the proposed method, the strain at Point A is artificially amplified. The specific method is as follows:

$$U_i'^A = \begin{cases} U_i^A, & i < 1600, \\ U_i^A \cdot \dfrac{(i-1600)}{492}\zeta, & i \geq 1600, \end{cases} \tag{45}$$

where U_i^A is the strain at the ith time point of point A before modification, $U_i'^A$ is the strain at the ith time point of Point A after modification, and ζ is the strain amplification factor, and is 0.25.

The state diagnosis results of the real bridge of the method based on PCA, the method based on the correlation model without a spatial window and the proposed method are shown in Figure 29.

As shown in Figure 29, when the strain amplification factor is 0.25, effective diagnosis of the condition of the real bridge can be achieved by using the proposed method. Compared with the proposed method, the method based on PCA and the method based on the correlation model without a spatial window has a lower diagnostic accuracy. When the strain amplification factor is 0.25, the summary

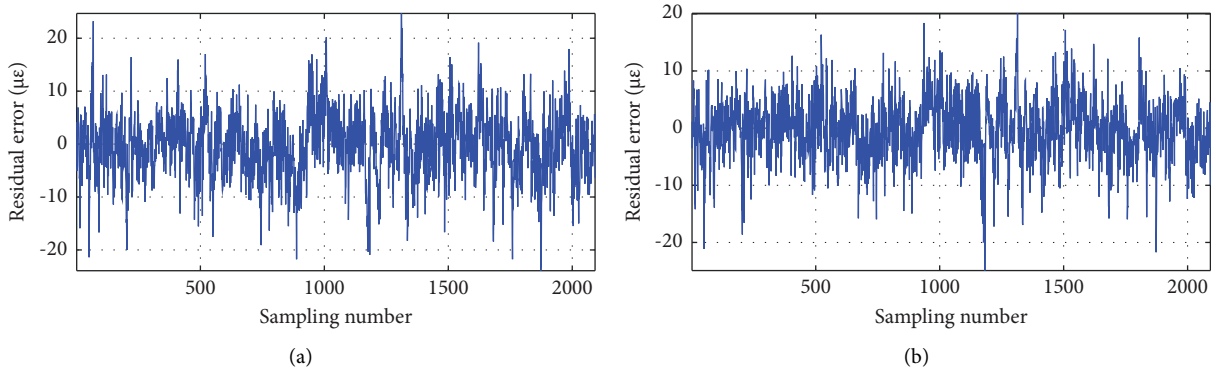

FIGURE 27: Residuals of the strain correlation model at the key point of the real bridge. (a) Key measured point *A* (b) Key measured point *B*.

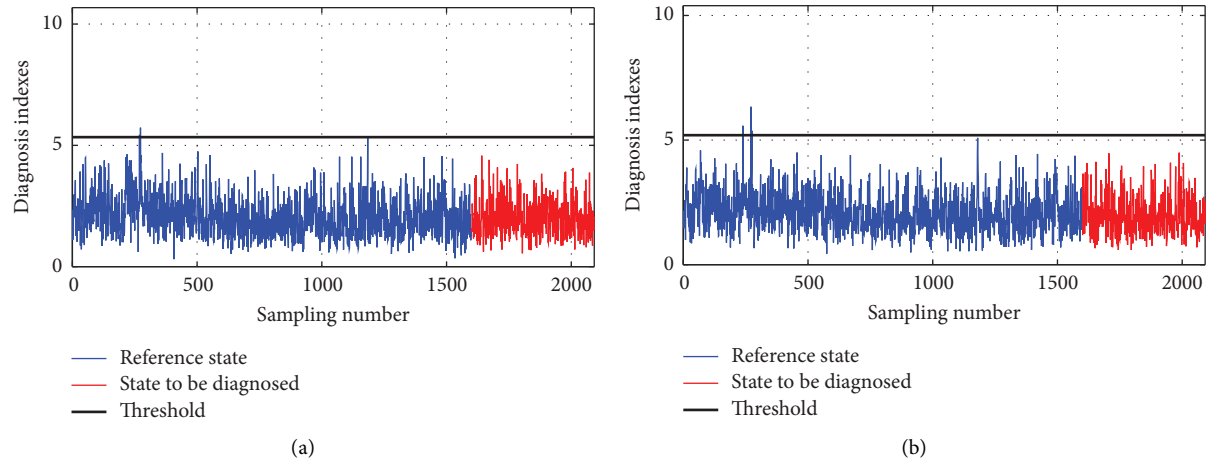

FIGURE 28: Results of the condition diagnosis of the real bridge. (a) Key measured point *A* (b) Key measured point *B*.

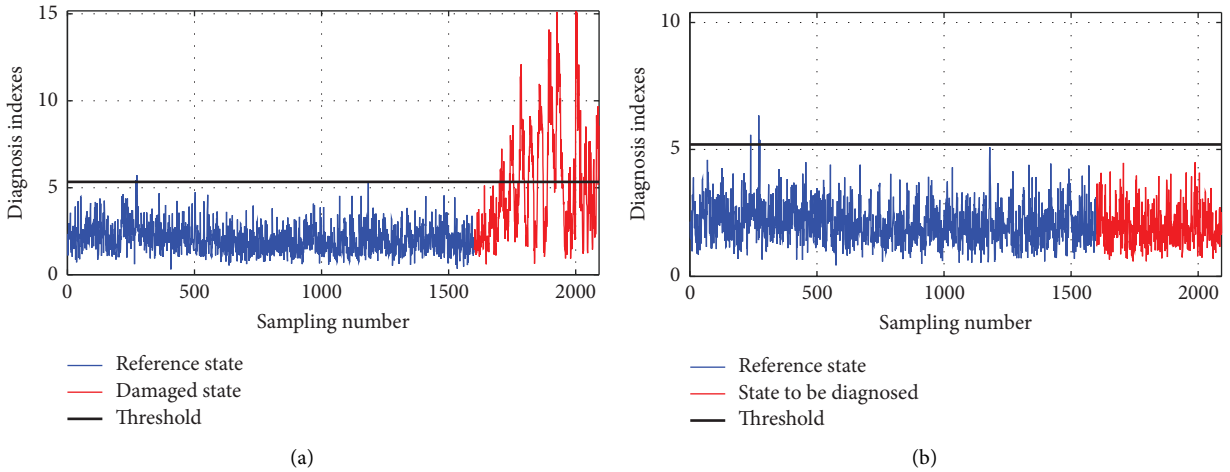

FIGURE 29: Continued.

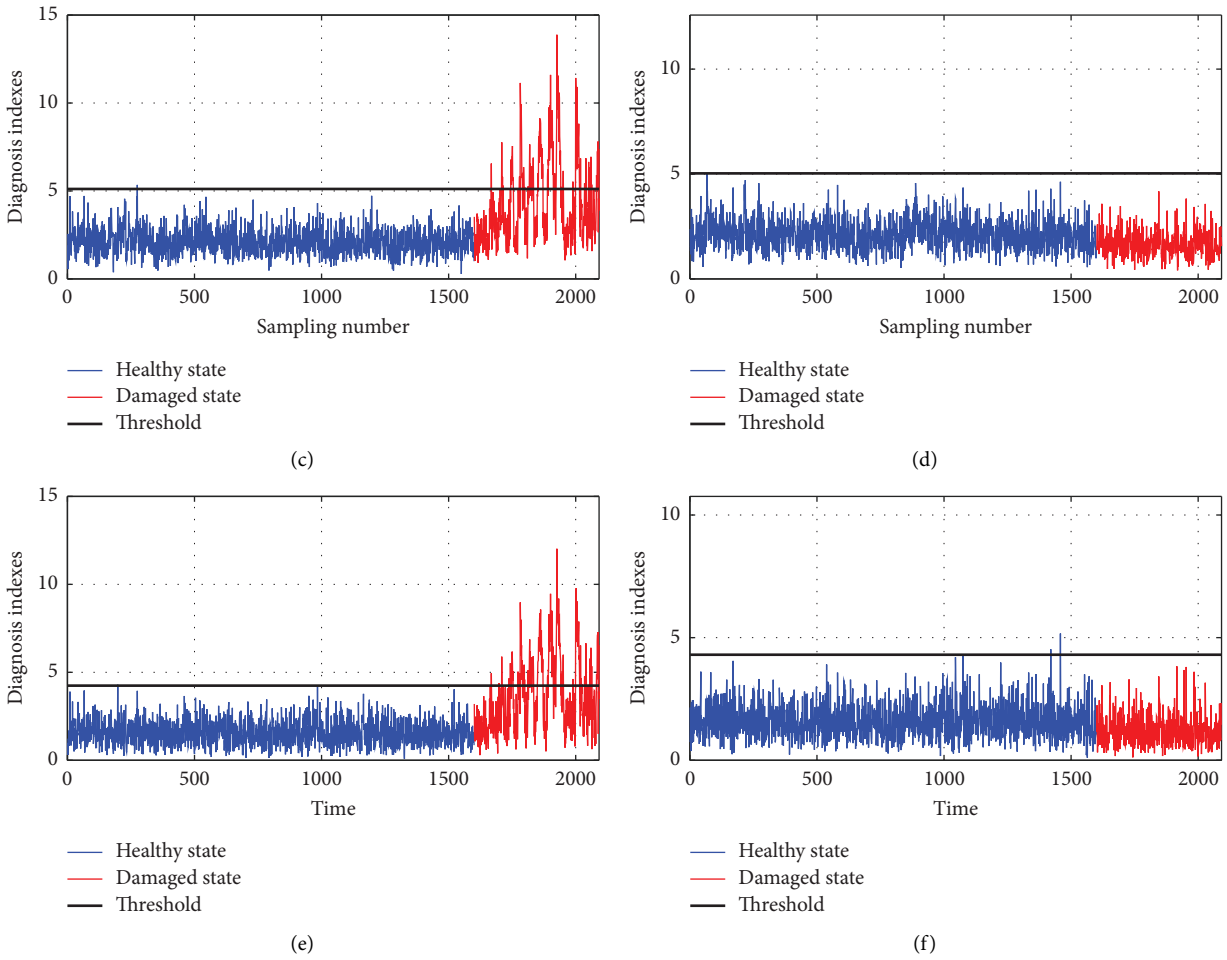

Figure 29: Results of the condition diagnosis of the real bridge after simulated damage is applied were obtained by using the proposed method and other methods. (a) Key measured point *A* (the proposed method). (b) Key measured point *B* (the proposed method). (c) Key measured point *A* (the method based on the correlation model without a spatial window). (d) Key measured point *B* (the method based on the correlation model without a spatial window). (e) Key measured point *A* (the method based on PCA). (f) Key measured point *B* (the method based on PCA).

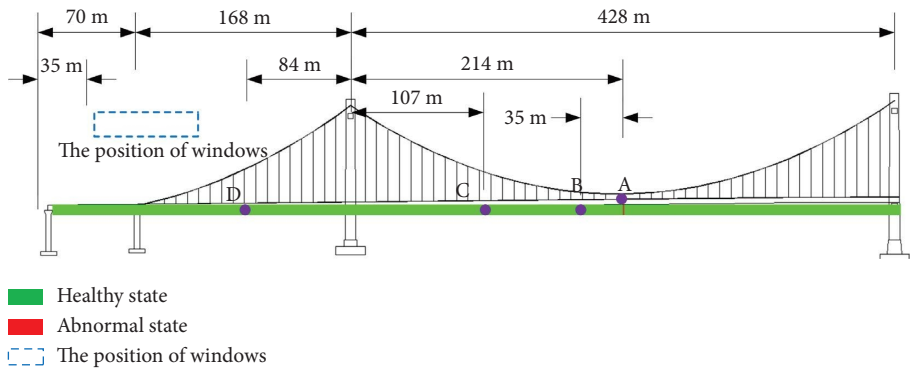

Figure 30: Summary diagnosis results of the real bridge (the strain amplification factor is 0.25, based on the strain correlation model for estimating the strain data of the left region by using the strain data of the right region in the spatial window).

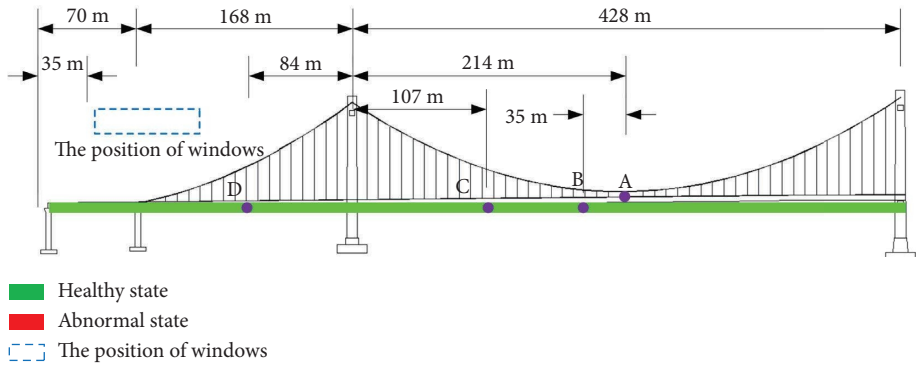

Figure 31: Summary diagnosis results of the real bridge (the strain amplification factor is 0.25, based on the strain correlation model for estimating the strain data of the right region by using the strain data of the left region in the spatial window).

diagnosis results of the real bridge are shown in Figures 30 and 31.

It can be seen from Figures 30 and 31 that the proposed method not only effectively identifies the occurrence of bridge damage but also accurately determines the abnormal strain region.

5. Conclusions

To diagnose the condition of a bridge by using the strain monitoring data from BOTDA sensors, a cross-diagnosis method for the structural condition of a long-span suspension bridge based on the spatial windows of distributed strain data is proposed. The following conclusions are developed as follows:

(1) Regarding one spatial window defined in this study, the correlation model between the distributed strain data of high-density measured points is effective in reducing the influence of ambient temperature on the results of the condition diagnoses of bridges.

(2) The numerical example and the example of a real bridge show that different load conditions of the bridge will lead to different degrees of correlation between the distributed strain data of high-density measured points and then lead to different division results of the spatial windows. Moreover, because the degree of correlation between the distributed strain data at different positions of the bridge is different under the coupling influence of various loads, it is not necessarily the best method to establish a correlation model by using the strain data of all measured points.

(3) The numerical example shows that the proposed method can effectively identify the occurrence of bridge damage and determine the damaged region; at the same time, the proposed method has a relatively strong ability to resist the interference of measured noise.

(4) The results of a numerical example and an example of a real bridge show that the diagnostic accuracy of the proposed method is higher than that of both the method based on the correlation model without a spatial window and the method based on PCA.

(5) The proposed method is only suitable for symmetric long-span bridges, and it is difficult to directly apply it to asymmetric bridges. In addition, regarding the bridge region that is not within the effective spatial window, the method based on PCA is recommended to diagnose the condition of the bridge.

Data Availability

The data used to support the findings of this study are available from the corresponding author upon request.

Conflicts of Interest

The authors declare that there are no conflicts of interest regarding the publication of this paper.

Acknowledgments

This study was supported by the Heilongjiang Provincial Key Research & Development Program (Grant no: GA21A303).

References

[1] J. Gosliga, D. Hester, K. Worden, and A. Bunce, "On population-based structural health monitoring for bridges," *Mechanical Systems and Signal Processing*, vol. 173, Article ID 108919, 2022.

[2] J. Cao and Y. Liu, "Damage localization for bridges monitored within one cluster based on a spatiotemporal correlation model of strain monitoring data," *Structural Health Monitoring*, vol. 22, no. 1, pp. 105–130, 2022.

[3] C. Yang, S. Zhang, Y. Liu, and K. Yu, "Damage detection of bridges under changing environmental temperature using the characteristics of the narrow dimension (cnd) of damage features," *Measurement*, vol. 189, Article ID 110640, 2022.

[4] Y. Liu and S. Zhang, "Probabilistic baseline of finite element model of bridges under environmental temperature changes," *Computer-Aided Civil and Infrastructure Engineering*, vol. 32, no. 7, pp. 581–598, 2017.

[5] H. Dai, R. Zhang, and M. Beer, "A new method for stochastic analysis of structures under limited observations," *Mechanical Systems and Signal Processing*, vol. 185, Article ID 109730, 2023.

[6] G. Zonno, R. Aguilar, R. Boroschek, and P. B. Lourenco, "Experimental analysis of the thermohygrometric effects on

the dynamic behavior of adobe systems," *Construction and Building Materials*, vol. 208, pp. 158–174, 2019.

[7] A. Entezami and H. Shariatmadar, "Damage localization under ambient excitations and non-stationary vibration signals by a new hybrid algorithm for feature extraction and multivariate distance correlation methods," *Structural Health Monitoring*, vol. 18, no. 2, pp. 347–375, 2019.

[8] M. H. Daneshvar, M. Saffarian, H. Jahangir, and H. Sarmadi, "Damage identification of structural systems by modal strain energy and an optimization-based iterative regularization method," *Engineering with Computers*, vol. 39, no. 3, pp. 2067–2087, 2022.

[9] J. He and Y. Zhou, "A novel mode shape reconstruction method for damage diagnosis of cracked beam," *Mechanical Systems and Signal Processing*, vol. 122, pp. 433–447, 2019.

[10] S. Jin and H. Jung, "Vibration-based damage detection using online learning algorithm for output-only structural health monitoring," *Structural Health Monitoring*, vol. 17, no. 4, pp. 727–746, 2018.

[11] T. Lin and Y. Chang, "Development of a real-time scour monitoring system for bridge safety evaluation," *Mechanical Systems and Signal Processing*, vol. 82, pp. 503–518, 2017.

[12] F. Xiao, J. L. Hulsey, and R. Balasubramanian, "Fiber optic health monitoring and temperature behavior of bridge in cold region," *Structural Control and Health Monitoring*, vol. 24, no. 11, Article ID e2020, 2017.

[13] X. Fan and Y. Liu, "Use of monitored daily extreme stress data for performance prediction of steel bridges: dynamic linear models and Gaussian mixed particle filter," *Mechanical Systems and Signal Processing*, vol. 121, pp. 841–855, 2019.

[14] S. Zhang and Y. Liu, "Damage detection of bridges monitored within one cluster based on the residual between the cumulative distribution functions of strain monitoring data," *Structural Health Monitoring*, vol. 19, no. 6, pp. 1764–1789, 2020.

[15] J. Cao, S. Zhang, and Y. Liu, "Probabilistic sddlv method for localizing damage in bridges monitored within one cluster under time-varying environmental temperatures," *Journal of Civil Structural Health Monitoring*, vol. 12, no. 1, pp. 47–70, 2022.

[16] J. Cao, Z. Zhou, and Y. Liu, "Damage localization for prefabricated bridges group using the area-ratio of the strain time-history curve," *Measurement*, vol. 198, Article ID 111172, 2022.

[17] J. Cao, Y. Liu, and C. Li, "Damage cross detection between bridges monitored within one cluster using the difference ratio of projected strain monitoring data," *Structural Health Monitoring*, vol. 21, no. 2, pp. 571–595, 2022.

[18] P. Ren and Z. Zhou, "Two-step approach to processing raw strain monitoring data for damage detection of structures under operational conditions," *Sensors*, vol. 21, no. 20, p. 6887, 2021.

[19] I. Farreras-Alcover, M. K. Chryssanthopoulos, and J. E. Andersen, "Regression models for structural health monitoring of welded bridge joints based on temperature, traffic and strain measurements," *Structural Health Monitoring*, vol. 14, no. 6, pp. 648–662, 2015.

[20] Y. Zhou and L. Sun, "A comprehensive study of the thermal response of a long-span cable-stayed bridge: from monitoring phenomena to underlying mechanisms," *Mechanical Systems and Signal Processing*, vol. 124, pp. 330–348, 2019.

[21] Y. Zhou and L. Sun, "Insights into temperature effects on structural deformation of a cable-stayed bridge based on structural health monitoring," *Structural Health Monitoring*, vol. 18, no. 3, pp. 778–791, 2019.

[22] T. Buckley, V. Pakrashi, and B. Ghosh, "A dynamic harmonic regression approach for bridge structural health monitoring," *Structural Health Monitoring*, vol. 20, no. 6, pp. 3150–3181, 2021.

[23] X. Lei, D. M. Siringoringo, Z. Sun, and Y. Fujino, "Displacement response estimation of a cable-stayed bridge subjected to various loading conditions with one-dimensional residual convolutional autoencoder method," *Structural Health Monitoring*, vol. 22, no. 3, pp. 1790–1806, 2022.

[24] A. Deraemaeker and K. Worden, "A comparison of linear approaches to filter out environmental effects in structural health monitoring," *Mechanical Systems and Signal Processing*, vol. 105, pp. 1–15, 2018.

[25] W. Soo Lon Wah, Y. Chen, G. W. Roberts, and A. Elamin, "Separating damage from environmental effects affecting civil structures for near real-time damage detection," *Structural Health Monitoring*, vol. 17, no. 4, pp. 850–868, 2018.

[26] M. Fallahian, F. Khoshnoudian, and V. Meruane, "Ensemble classification method for structural damage assessment under varying temperature," *Structural Health Monitoring*, vol. 17, no. 4, pp. 747–762, 2018.

[27] K. Erazo, D. Sen, S. Nagarajaiah, and L. Sun, "Vibration-based structural health monitoring under changing environmental conditions using kalman filtering," *Mechanical Systems and Signal Processing*, vol. 117, pp. 1–15, 2019.

[28] Y. Xu, Y. Tian, and H. Li, "Unsupervised deep learning method for bridge condition assessment based on intra-and inter-class probabilistic correlations of quasi-static responses," *Structural Health Monitoring*, vol. 22, no. 1, pp. 600–620, 2022.

[29] X. Bao, D. J. Webb, and D. A. Jackson, "22-km distributed temperature sensor using Brillouin gain in an optical fiber," *Optics Letters*, vol. 18, no. 7, pp. 552–554, 1993.

[30] Y. Dong, H. Zhang, L. Chen, and X. Bao, "2 cm spatial-resolution and 2 km range Brillouin optical fiber sensor using a transient differential pulse pair," *Applied Optics*, vol. 51, no. 9, pp. 1229–1235, 2012.

[31] Y. Peled, A. Motil, and M. Tur, "Fast Brillouin optical time domain analysis for dynamic sensing," *Optics Express*, vol. 20, no. 8, pp. 8584–8591, 2012.

[32] D. Ba, D. Zhou, B. Wang et al., "Dynamic distributed Brillouin optical fiber sensing based on dual-modulation by combining single frequency modulation and frequency-agility modulation," *IEEE Photonics Journal*, vol. 9, no. 3, pp. 1–8, 2017.

[33] F. Ansari, "Fiber optic health monitoring of civil structures using long gage and acoustic sensors," *Smart Materials and Structures*, vol. 14, no. 3, pp. S1–S7, 2005.

[34] X. Feng, X. Zhang, C. Sun, M. Motamedi, and F. Ansari, "Stationary wavelet transform method for distributed detection of damage by fiber-optic sensors," *Journal of Engineering Mechanics*, vol. 140, no. 4, Article ID 040130044, 2014.

[35] E. A. Oskoui, T. Taylor, and F. Ansari, "Method and monitoring approach for distributed detection of damage in multi-span continuous bridges," *Engineering Structures*, vol. 189, pp. 385–395, 2019.

[36] W. Zhang, B. Shi, Y. Zhang, J. Liu, and Y. Zhu, "The strain field method for structural damage identification using Brillouin optical fiber sensing," *Smart Materials and Structures*, vol. 16, no. 3, pp. 843–850, 2007.

[37] S. Wei, Z. Zhang, S. Li, and H. Li, "Strain features and condition assessment of orthotropic steel deck cable-

supported bridges subjected to vehicle loads by using dense fbg strain sensors," *Smart Materials and Structures*, vol. 26, no. 10, Article ID 104007, 2017.

[38] A. Scarella, G. Salamone, S. K. Babanajad, A. De Stefano, and F. Ansari, "Dynamic Brillouin scattering-based condition assessment of cables in cable-stayed bridges," *Journal of Bridge Engineering*, vol. 22, no. 3, Article ID 040161303, 2017.

[39] E. A. Oskoui, T. Taylor, and F. Ansari, "Reference-free dynamic distributed monitoring of damage in multispan bridges," *Journal of Structural Engineering*, vol. 147, no. 1, 2021.

[40] F. Ansari and Y. Libo, "Mechanics of bond and interface shear transfer in optical fiber sensors," *Journal of Engineering Mechanics*, vol. 124, no. 4, pp. 385–394, 1998.

[41] S. Her and C. Huang, "Effect of coating on the strain transfer of optical fiber sensors," *Sensors*, vol. 11, no. 7, pp. 6926–6941, 2011.

[42] X. Feng, J. Zhou, C. Sun, X. Zhang, and F. Ansari, "Theoretical and experimental investigations into crack detection with botdr-distributed fiber optic sensors," *Journal of Engineering Mechanics*, vol. 139, no. 12, pp. 1797–1807, 2013.

[43] H. Wang and J. Dai, "Strain transfer analysis of fiber Bragg grating sensor assembled composite structures subjected to thermal loading," *Composites Part B: Engineering*, vol. 162, pp. 303–313, 2019.

[44] F. Liu, Q. Xu, and Y. Liu, "Strain data correction of distributed optical fiber sensors using strain transfer model with variable shear lag parameters," *Automation in Construction*, vol. 140, Article ID 104311, 2022.

[45] H. W. Zhao, Y. L. Ding, A. Q. Li, Z. Z. Ren, and K. Yang, "Live-load strain evaluation of the prestressed concrete box-girder bridge using deep learning and clustering," *Structural Health Monitoring*, vol. 19, no. 4, pp. 1051–1063, 2020.

[46] H. W. Zhao, Y. L. Ding, A. Q. Li, B. Chen, and K. P. Wang, "Digital modeling approach of distributional mapping from structural temperature field to temperature-induced strain field for bridges," *Journal of Civil Structural Health Monitoring*, vol. 13, no. 1, pp. 251–267, 2023.

[47] D. N. Reshef, Y. A. Reshef, H. K. Finucane et al., "Detecting novel associations in large data sets," *Science*, vol. 334, no. 6062, pp. 1518–1524, 2011.

[48] V. Badrinarayanan, A. Kendall, and R. Cipolla, "Segnet: a deep convolutional encoder-decoder architecture for image segmentation," *IEEE Transactions on Pattern Analysis and Machine Intelligence*, vol. 39, no. 12, pp. 2481–2495, 2017.

[49] R. De Maesschalck, D. Jouan-Rimbaud, and D. L. Massart, "The mahalanobis distance," *Chemometrics and Intelligent Laboratory Systems*, vol. 50, no. 1, pp. 1–18, 2000.

[50] B. Chen, Z. Ye, Z. Chen, and X. Xie, "Bridge vehicle load model on different grades of roads in China based on Weigh-in-Motion (WIM) data," *Measurement*, vol. 122, pp. 670–678, 2018.

[51] H. W. Zhao, Y. L. Ding, A. Q. Li, W. Sheng, and F. F. Geng, "Digital modeling on the nonlinear mapping between multi-source monitoring data of in-service bridges," *Structural Control and Health Monitoring*, vol. 27, no. 11, pp. 1–17, 2020.

[52] H. W. Zhao, Y. L. Ding, A. Q. Li, X. W. Liu, B. Chen, and J. Lu, "Evaluation and early warning of vortex-induced vibration of existed long-span suspension bridge using multisource monitoring data," *Journal of Performance of Constructed Facilities*, vol. 35, no. 3, Article ID 04021007, 2021.